Journal of Materials Chemistry A

FEATURE ARTICLE

View Article Online
View Journal

Flexible supercapacitors based on carbon nanomaterials

Cite this: DOI: 10.1039/c4ta00567h

Tao Chen and Liming Dai*

Flexible energy storage devices are essential for the development of flexible and wearable electronics. Flexible supercapacitors (also known as electrochemical capacitors or ultracapacitors) have attracted increasing attention for advanced energy storage because of their high capability, long cycle life, low cost, and easy fabrication. Carbon nanomaterials, including 1D carbon nanotubes, 2D graphene, and 3D mesoporous carbon, are promising as electrode materials for flexible supercapacitors due to their extremely large surface area, excellent mechanical and electrical properties, and high electrochemical stability. Much effort has been devoted to developing flexible, carbon-based, all-solid-state supercapacitors with different structure/performance characteristics, including conventional planar, ultrathin in-plane, wearable fiber-shaped, stretchable, transparent, and integrated devices with aesthetic appeal. The aim of this article is to provide an overview of recent progress towards the development of advanced flexible supercapacitors based on carbon nanomaterials. The challenges and perspectives in this emerging field are also discussed.

Received 31st January 2014
Accepted 24th February 2014

DOI: 10.1039/c4ta00567h

www.rsc.org/MaterialsA

1 Introduction

1.1 Background of electrochemical capacitors

The increasing depletion of fossil fuels and the environmental problems associated with their use have inspired the development of new types of clean and sustainable energy conversion systems (*e.g.*, solar, wind, and water splitting) as new power sources with low exhaust emissions for transportation and stationary applications. As these new energy forms are often limited by time (*e.g.*, solar and wind) or region (*e.g.*, water), energy storage systems, such as supercapacitors (also known as electrochemical capacitors or ultracapacitors) and batteries, are required to ensure continued and balanced power supplies. Although supercapacitors possess a relatively low energy density with respect to batteries (*e.g.*, lithium-ion batteries), supercapacitors have received intensive attention for decades due to

Center of Advanced Science and Engineering for Carbon (Case4Carbon), Department of Macromolecular Science and Engineering, Case Western Reserve University, 10900 Euclid Avenue, Cleveland, OH 44106, USA. E-mail: liming.dai@case.edu

Tao Chen is currently a postdoctoral fellow in the Department of Macromolecular Science and Engineering at CWRU. He received his BS and MS in the Science of Polymer Materials from Zhengzhou University in 2006 and 2009, respectively, and received a PhD in Macromolecular Chemistry and Physics from Fudan University in 2012. His research interests focus on the design and fabrication of carbon nanomaterials for flexible, wearable and stretchable energy conversion, storage and their integrated devices.

Liming Dai joined CWRU in 2009 as the Kent Hale Smith Professor in the Department of Macromolecular Science and Engineering. He is also director of Case4Carbon. He received a BSc from Zhejiang University in 1983 and a PhD from the Australian National University in 1991. He was a postdoctoral fellow at the University of Cambridge, a visiting fellow at the University of Illinois, and spent 10 years with CSIRO in Australia. He was a professor at the University of Akron and at the University of Dayton. His expertise is the synthesis, chemical modification, and device fabrication of conjugated polymers and carbon nanomaterials for energy and bio-related applications.

their high power density (up to 10 kW kg^{-1}) and fast charging (in seconds, Fig. 1)[1,2] attractive for various applications, including energy sources for hybrid electrical vehicles, power back-up in portable electronics, load-leveling and other successive power supplies.[3]

According to the energy storage mechanism and the nature of the electrode material, supercapacitors can be classified into three types:[3–5] (i) electrical double-layer capacitors (EDLCs), in which the electrostatic charge accumulates at the interface between the electrode surface and the electrolyte, (ii) pseudocapacitors with fast and reversible redox reactions (Faradaic processes) occurring on the surface of electrodes, and (iii) hybrid capacitors in which both the EDLC and pseudocapacitor work together in a single device. In EDLCs, the electrode surface area plays a crucial role in the performance of a capacitor. Carbon materials with large specific surface areas, such as activated carbon,[6,7] carbon nanofibers,[8,9] mesoporous carbon,[10,11] carbon nanotubes,[12,13] graphene,[14–16] and carbide-derived carbon,[17,18] have been widely employed in EDLCs. In an EDLC, electrical energy is stored through ion adsorption (a purely electrostatic process) without Faradic charge transfer, leading to high power densities, fast charge–discharge processes, and excellent cycling stabilities. However, the limited surface area and pore size distribution of conventional electrode materials often cause relatively low energy densities (normally, <10 W h kg^{-1}).[2,13] In this context, pseudocapacitors have been developed to increase the energy densities. In pseudocapacitors, composite materials composed of carbon nanomaterials together with electrically conductive polymers (*e.g.*, polyaniline,[19,20] polypyrrole,[21,22] and poly[3,4-ethylenedioxythiophene][23]) or transition metal oxides (*e.g.*, MnO_2,[24,25] NiO,[26] RuO_2,[27] V_2O_5 (ref. 28) and TiO_2 (ref. 25)) have been widely used for the electrodes. Due to the structural instability intrinsically associated with conductive polymers, pseudocapacitors usually have a short cycle life. On the other hand, the limited electrical conductivity and intrinsic rigidity of metal oxides often leads to low power density and poor flexibility. To achieve high electrochemical performance and good mechanical stability for flexible supercapacitors, therefore, hybrid capacitors based on composites of carbon nanomaterials and electroactive polymers have been developed.[2]

1.2 Performance evaluation of supercapacitors

For a typical EDLC, charge accumulated at the electrode–electrolyte interface, and hence capacitance, is generally defined by eqn (1) for a parallel-plated capacitor[7,29,30]

$$C = \frac{\varepsilon_0 \varepsilon_r A}{D} \quad (1)$$

where ε_0 is the permittivity of free space, ε_r is the dielectric constant of an electrolyte, A is the specific surface area of the electrode, and D is the distance between the two electrodes. Therefore, the capacitance of an EDLC capacitor depends strongly on the electrode surface area, separation distance between the two electrodes, and properties of the electrolyte.

Generally speaking, an EDLC (Fig. 2a and b) consists of two electrodes separated by an ion-permeable separator in an electrolyte to prevent short-circuit. In the charged state, the electrolyte anions and cations move towards the positive and negative electrodes, respectively, to generate an electrical double-layer at each of the two electrode–electrolyte interfaces in the EDLC. As a result, a complete cell can be considered as two capacitors connected in series as each of the electrode–electrolyte interfaces represents a capacitor. Therefore, the cell capacitance (C_{cell}) of a capacitor can be calculated according to eqn (2):[4,7]

$$\frac{1}{C_{cell}} = \frac{1}{C_+} + \frac{1}{C_-} \quad (2)$$

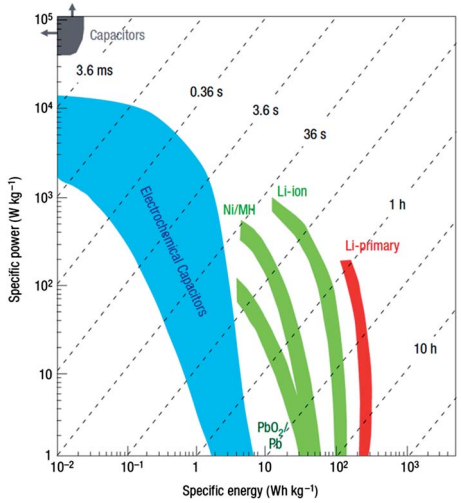

Fig. 1 Ragone plot for various electrical energy storage devices.[2] Reprinted from ref. 2 with permission. Copyright 2008, Nature Publishing Group.

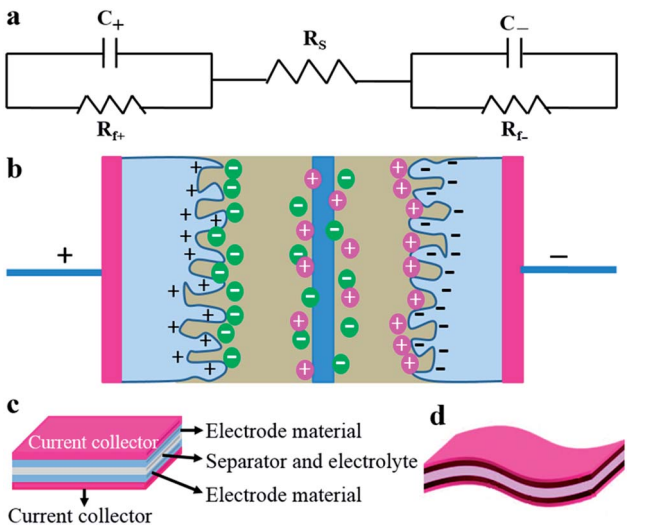

Fig. 2 (a) Equivalent circuit model for an electrochemical capacitor. (b) Schematic representation of a two-electrode supercapacitor. (c and d) Schematic illustrations of the typical structure of a conventional supercapacitor (c) and its flexible counterpart (d).

where, C_+ and C_- represent the capacitance of the positive and negative electrodes, respectively.[29] In the case of a symmetric device, the capacitance of the positive electrode (C_+) must equal that of the negative one (C_-), thus the capacitance of the complete cell is half of the capacitance of each individual electrode, that is,[4,7]

$$C_{\text{cell}} = \frac{C_e}{2} \tag{3}$$

where $C_e = C_+ = C_-$.

In addition to capacitance, energy and power densities are the other two important parameters for evaluating the electrochemical performance of a supercapacitor. The energy density measures the capacity to perform work while the power density is the rate of energy delivery per unit time. Cyclic voltammetry (CV), galvanostatic charge–discharge (GCD) and electrochemical impedance spectroscopy (EIS) are the three most frequently used techniques for characterizing the electrochemical performance of a supercapacitor. Supercapacitors without Faradaic reaction between the active electrode materials and electrolytes (*i.e.*, EDLCs) can show rectangularly-shaped CV curves whereas redox peaks are observable for pseudocapacitors. The specific capacitance of a supercapacitor cell can also be calculated by using the voltammetric charge integrated from a CV curve according to eqn (4),[4]

$$C_{\text{cell}} = \frac{Q}{2mV} = \frac{1}{2mv}\int_{V_-}^{V_+} I(V)\mathrm{d}V \tag{4}$$

where C_{cell} (in F g^{-1}) is the specific capacitance of the cell, Q (in coulomb, C) is the total charge obtained by integrating the positive and negative sweeps in a CV curve, m (in grams, g) is the mass of the active materials in both the electrodes (if the area or volume is more important for specific applications, m can be substituted by the electrode area or volume), v (in V s^{-1}) is the scan rate, and $V = V_+ - V_-$, is the potential window between the positive (V_+) and negative (V_-) electrodes. At a constant scan rate v, the average specific power density (P, in W kg^{-1}) during discharge can be calculated by integrating the CV curves using eqn (5),[4]

$$P = \frac{1}{mV}\int_0^{V_+} IV\mathrm{d}V \tag{5}$$

where V is the initial voltage during discharge and m is the total mass of both the electrodes. The specific energy density (E, in W h kg^{-1}) can be calculated according to eqn (6),[4]

$$E = \frac{1}{3600mv}\int_0^{V_+} IV\mathrm{d}V \tag{6}$$

For the GCD method, the cell capacitance of a supercapacitor can be calculated from the charge–discharge curve according to eqn (7),[4]

$$C_{\text{cell}} = \frac{I}{m\mathrm{d}V/\mathrm{d}t} \tag{7}$$

in which I (in A) is the discharge current, m (in g) is the total mass of the active materials in the two electrodes, $\mathrm{d}V/\mathrm{d}t$ is the slope of the discharge curve. The initial portion of a discharge curve often has a very short IR drop due to the internal resistance. The rest of the discharge curve is typically linear for non-Faradic materials, while large deviations in linearity could occur for pseudocapacitors and hybrid systems. In order to avoid overestimation of the specific capacitance, $\mathrm{d}V/\mathrm{d}t$ may be calculated from eqn (8),[31]

$$\mathrm{d}V/\mathrm{d}t = \left(V_{\max} - \frac{V_{\max}}{2}\right)\Big/(T_2 - T_1) \tag{8}$$

where $V_{\max}$ is the potential after the IR drop, T_2 and T_1 are the corresponding discharge times of $V_{\max}$ and $V_{\max}/2$.

It is important to note that the specific capacitance for electrode materials is usually derived from three-electrode measurements involving the reference and counter electrodes.[4,31] This value is much higher than the actual cell capacitance from a two-electrode measurement. Typically, the specific capacitance for one single electrode C_{one} (F g^{-1}) is calculated according to eqn (9),[4,31]

$$C_{\text{one}} = 4C_{\text{cell}} \tag{9}$$

where C_{cell} is the specific cell capacitance for the two-electrode supercapacitor calculated from the CV curve or charge–discharge curve.

From the total specific cell capacitance of a two-electrode system (C_{cell}), the maximum energy ($E_{\max}$, in W h kg^{-1}) and maximum power ($P_{\max}$, in W kg^{-1}) of a supercapacitor cell can be calculated according to eqn (10) and (11), respectively,[4,31]

$$E_{\max} = \frac{1}{2}C_{\text{cell}}V^2 \tag{10}$$

$$P_{\max} = \frac{V^2}{4R_s} \tag{11}$$

where, V is the cell voltage, and R_s is the total equivalent series resistance (ESR) of the supercapacitor. Therefore, a high-performance supercapacitor must have a large capacitance, high cell operating voltage, and minimum equivalent series resistance.

1.3 Carbon nanomaterials for flexible supercapacitors

Flexible energy storage devices (*e.g.*, supercapacitors, Fig. 2d) have recently attracted a great deal of interest for their potential applications in various flexible electronic systems, including roll-up and bendable displays, portable electronic papers, and wearable personal multi-media.[32–34] Consequently, some flexible all-solid-state supercapacitors have been developed by sandwiching gel electrolyte (*e.g.*, polyvinyl alcohol, PVA, and H_3PO_4 or H_2SO_4 gels) between positive/negative electrodes supported with flexible plastic substrates (*e.g.*, polydimethylsiloxane, PDMS).[34–36] Unlike conventional supercapacitors with liquid electrolytes, the solid-state gel electrolytes used in flexible supercapacitors act as both the electrolyte and separator to avoid short circuit and chemical leakage.

Owing to their large surface area, excellent electrical, mechanical, and electrochemical properties, carbon

nanomaterials (especially, carbon nanotubes, CNTs, and graphene sheets) have been widely used as active materials/electrodes in (flexible) supercapacitors.[13,34,37–39] These earlier studies have demonstrated that carbon nanomaterials are promising for the development of supercapacitors in general and flexible supercapacitors in particular. Several recent reviews for supercapacitors based on carbon nanomaterials have appeared,[34,38–40] and interested readers can obtain more detailed information from appropriate references cited for various specific carbon electrodes, including carbon nanomaterials,[5,13,15,16,40,41] porous carbon,[42] conductive polymers,[43,44] and 3D nanostructured carbon.[39] However, the progresses on carbon-based flexible supercapacitors has been much less discussed in the literature.[34] The aim of this article is to provide a comprehensive review of various newly-developed flexible all-solid-state supercapacitors based on carbon nanomaterials (Fig. 3), including in-plane,[45] fiber-shaped,[46] stretchable,[47] transparent and integrated supercapacitors.[48] In what follows, we first describe nanocarbon-based flexible (micro-) supercapacitors with planar structures. Then, we illustrate wearable fiber-shaped supercapacitors based on carbon nanomaterials, followed by carbon-based stretchable and transparent supercapacitors. Finally, flexible supercapacitors integrated with other energy devices will be discussed, along with challenges and perspectives in this emerging field.

2 Nanocarbon-based flexible supercapacitors with planar structures

The 1D CNTs and 2D graphene represent two of the most extensively exploited carbon allotropes for electrochemical energy storage.[33,34] High-performance flexible supercapacitors with planar structures based on CNT, graphene, and their hybrid electrodes have been developed, and are the subject of this section.

2.1 CNT-based flexible supercapacitors

CNTs have been widely used as electrode materials in flexible supercapacitors with both liquid electrolyte and gel electrolyte.[13,33] For this purpose, CNTs can be brush-/spray-coated directly onto either flexible nonconductive substrates (*e.g.*, plastic film, cellulose paper, and office paper) as both the current electrode and current collector,[57–60] or flexible conductive substrates (*e.g.*, metal coated plastic films) as electrode materials.[61,62] In this regard, Kaempgen and co-workers[57] reported printable thin film supercapacitors using spray-coated single-walled CNTs on polyethylene-therephthalate (PET) films (Fig. 4a) as both electrodes and charge collectors. In order to make the device fully printable, gel electrolyte (PVA/H_3PO_4) was used to combine the separator and electrolyte into a single layer. The CNT electrodes and the gel electrolyte were sandwiched together, leading to the thin film supercapacitors (Fig. 4b). Fig. 4c and d show the CV and GCD curves of the-solid-state supercapacitors thus prepared, from which a specific capacitance of $\sim$36 F g^{-1} was obtained. Apart from the plastic films, other low-cost light-weight substrates (*e.g.*, office paper, bacterial nanocellulose) onto which CNTs have been deposited have also been used as electrodes in flexible supercapacitors.[59,60] For instance, Kang *et al.* deposited CNTs onto a bacterial nanocellulose substrate through a vacuum filtering process, and the resultant papers showed a high flexibility, large specific surface area, and good chemical stability.[60] The assembled all-solid-state flexible supercapacitors exhibited a high specific capacitance of 46.9 F g^{-1} at a scan rate of 0.1 V s^{-1}, and an excellent stability with a less than 0.5% loss of capacitance after 5000 charge–discharge cycles at a high current density of 10 A g^{-1}.

In order to further improve the performance of the pristine CNT-based flexible EDLCs, CNT composites with transition metal oxides and/or conductive polymers have been used to introduce pseudocapacitance into the flexible supercapacitors.[63–66] In particular, Meng *et al.*,[67] have reported a flexible all-solid-state supercapacitor using paper-like PANI-coated CNT networks (Fig. 4e) as the electrodes. A high specific capacitance of 350 F g^{-1} was obtained for the electrode materials (Fig. 4f and g) and 31.4 F g^{-1} for the entire device, which showed a good stability with only 8.1% decay in specific capacitance over 1000 charge–discharge cycles.

The free-standing randomly distributed CNT-based electrodes had high resistances and a complicated pore structure (micro-pores), which caused slow ion transport. Unlike random CNT networks, vertically-aligned CNTs (VA-CNTs) can create an aligned porous structure with well-defined inter-tube spacing to provide a larger electrolyte-accessible surface for efficient charge storage/delivery.[68–71] Theoretical simulation and experimental results have proved that supercapacitors based on the VA-CNTs exhibited a higher rate capability (the capability of discharging 50% of its stored energy in less than 0.76 ms) than that of supercapacitors based on random CNT networks.[70] Moreover, the top end-caps of VA-CNTs can be properly opened through appropriate methods (*e.g.*, by plasma etching[72,73]), allowing the electrolyte access to the otherwise inaccessible inner cavity of the VA-CNTs for additional charge storage. As expected, recent research has indicated that ther improved rate capability of VA-CNTs over random CNTs can be achieved for a three-electrode system using a liquid electrolyte.[68,72,74–76] Specifically, a high capacitance of 365 F g^{-1} has been obtained in 1 M H_2SO_4 for a VA-CNT array electrode prepared by template-assisted CVD[75] and 440 F g^{-1} for a VA-CNT electrode in ionic liquid electrolytes[62] prepared by a template-free CVD approach.[72,76] However, VA-CNTs, either with their tip opened or closed, have hardly been exploited for applications in two-electrode all-solid-state supercapacitors, which would surely further enhance the performance of the flexible device.

2.2 Graphene-based flexible supercapacitors

As a building block for all other graphitic carbon forms, including CNTs, graphene has been used for various potential applications where CNTs have been exploited. Having many similarities to CNTs, including a large specific surface area, good electronic and mechanical properties, and chemical stability,[37,77–79] graphene has also been investigated for use as

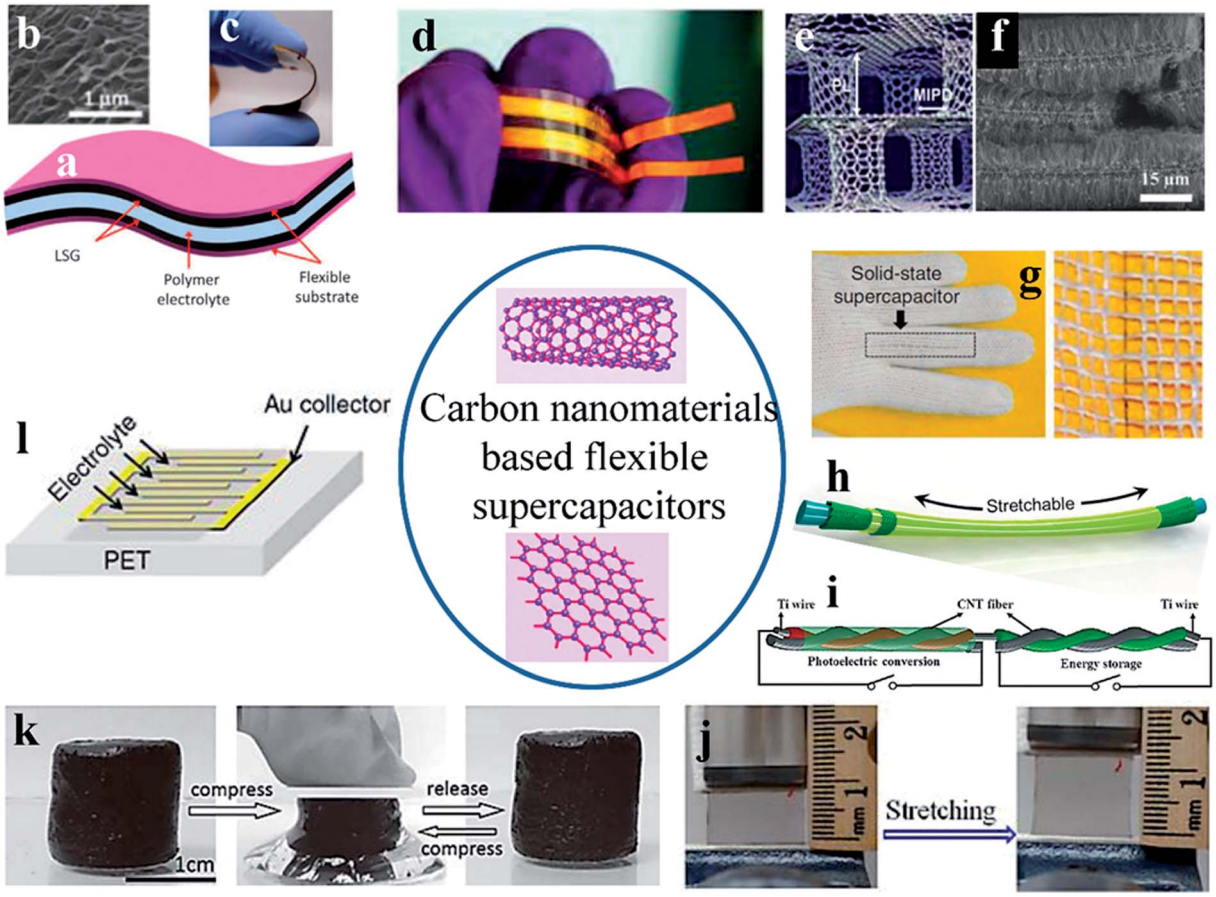

Fig. 3 An overview of various flexible all-solid-state supercapacitors based on carbon nanomaterials of different structures and forms: (a–c) graphene-based supercapacitor with a planar structure.[49] Reproduced from ref. 49 with permission. Copyright 2012, AAAS. (d) Graphene-based ultrathin supercapacitor.[50] Reproduced from ref. 50 with permission. Copyright 2011. American Chemical Society. (e and f) 3D CNT/graphene architectures for supercapacitors.[51] Reproduced from ref. 51 with permission. Copyright 2011. American Chemical Society. (g) Wearable fiber-shaped supercapacitor.[52] Reprinted from ref. 52 with permission. Copyright 2013, Nature Publishing Group. (h) Stretchable fiber-shaped supercapacitor.[53] Reproduced from ref. 53 with permission. Copyright 2013, John Wiley and Sons. (i) Integrated energy conversion and storage device in a wire.[54] Reproduced from ref. 54 with permission. Copyright 2012, John Wiley and Sons. (j) Graphene-based transparent and stretchable supercapacitor.[55] Reproduced from ref. 55 with permission. Copyright 2014. American Chemical Society. (k) 3D graphene composite for compressible supercapacitor.[56] Reproduced from ref. 56 with permission. Copyright 2013, John Wiley and Sons. (l) Microsupercapacitor with in-plane structure.[45] Reproduced from ref. 45 with permission. Copyright 2013, Nature Publishing Group.

electrodes in supercapacitors.[15,16,23,41,45] Various approaches, including chemical reduction from graphene oxide (GO),[80–82] chemical vapor deposition,[83] and a ball milling approach,[84] have been developed to produce graphene. The resultant graphene materials have been widely used as electrodes in supercapacitors based on liquid electrolytes.[15,41,85] Of particular interest, a capacitance of 200 F g^{-1} for a single electrode has been achieved from two-electrode supercapacitors using graphene electrode materials with a high surface area (3100 m^2 g^{-1}) produced by chemical activation.[85]

Along with the development of graphene-based supercapacitors involving liquid electrolytes, flexible all-solid-state supercapacitors based on graphene electrodes have also been reported to show many interesting results.[36,49,86,87] For instance, El-Kady *et al.*,[49] used a standard LightScribe DVD optical drive for laser-induced reduction of graphite oxide films to produce graphene electrodes for supercapacitors without the need for a binder or current collector (Fig. 5a–f). Flexible all-solid-state supercapacitors thus prepared showed a high power density (20 W cm^{-3}, 20 times higher than that of the activated carbon counterpart), energy density (1.36 mW h cm^{-3}, 2 times higher than that of the activated carbon counterpart), and excellent stability even under bending from 0 to 180° (Fig. 5g–i).

The reported specific capacitances for most solid-state supercapacitors based on free-standing graphene materials are in the range from 80 to 118 F g^{-1}, which is much lower than the corresponding theoretical value (550 F g^{-1}),[88] due to the restacking of graphene sheets to reduce the active surface area of the graphene materials and slowing down of the ion transport/diffusion within the active materials. To overcome this limitation, porous 3D graphene networks, such as graphene hydrogels and aerogels, have been devised as efficient electrodes in electrochemical energy storage devices.[89–96] Such porous 3D graphene materials have been prepared by freeze

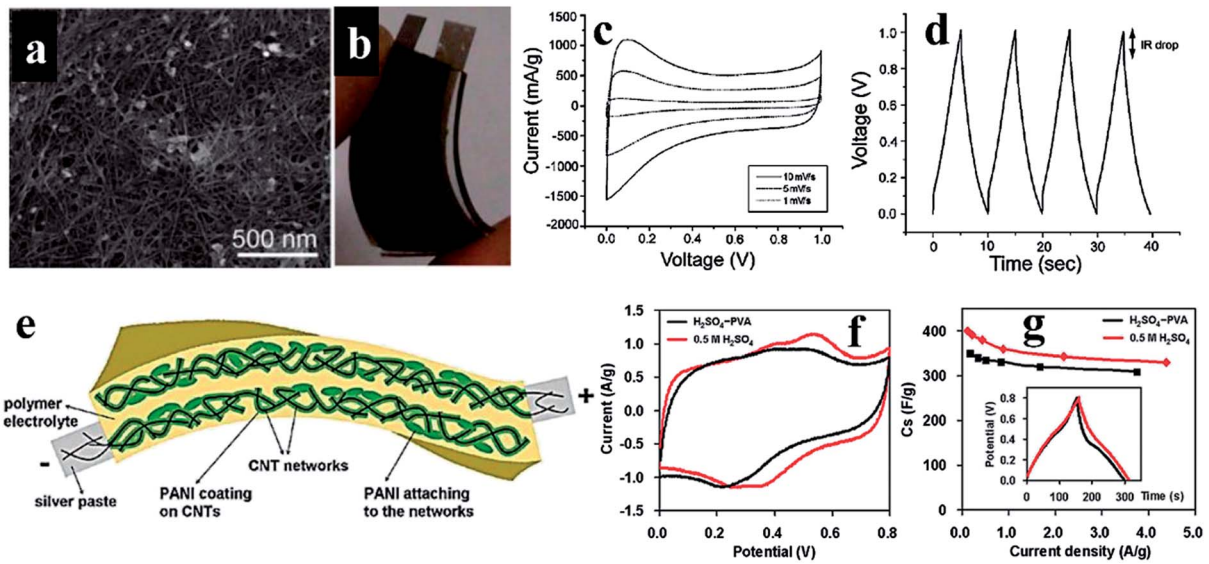

Fig. 4 (a) SEM image of the as-deposited SWCNT networks. (b) Thin film supercapacitor using sprayed SWCNT films on PET as the electrodes and a PVA/H_3PO_4 based polymer electrolyte as both the electrolyte and separator. (c and d) CV (c) and GCD (d) curves of the thin film supercapacitor.[57] Reproduced from ref. 57 with permission. Copyright 2009. American Chemical Society. (e) Schematic illustration of the PANI/CNT nanocomposite electrode well solidified in the polymer gel electrolyte. (f and g) Comparison of cyclic voltammetry at 5 mV s^{-1} (f) and discharge abilities (g) of the flexible PANI/CNT nanocomposite thin film electrodes in the H_2SO_4–PVA gel electrolyte and in the 0.5 M H_2SO_4 aqueous solution. The inset in (g) shows one cycle of the galvanostatic charge–discharge curves at 1 A g^{-1} in the H_2SO_4–PVA gel electrolyte and in the 0.5 M H_2SO_4 aqueous solution.[67] Reproduced from ref. 67 with permission. Copyright 2010. American Chemical Society.

drying a chemically-reduced GO dispersion[96] or direct chemical vapor deposition on nickel foam.[89,97] In both cases, the restacking of graphene sheets has been efficiently prevented and the diffusion of electrolytes through the graphene network was greatly facilitated. As a result, supercapacitors (three-electrode) based on 3D graphene hydrogels showed an improved electrochemical performance with specific capacitances of up to 220 F g^{-1} for a single electrode at 1 A g^{-1} in 5 M KOH aqueous solution.[92] Flexible all-solid-state supercapacitors using 3D graphene hydrogel films as the electrodes (Fig. 6a–c) with a high gravimetric specific capacitance (186 F g^{-1} at 1 A g^{-1}, area-specific capacitance of 372 mF cm^{-2}), excellent rate capability (70% retention at 20 A g^{-1}), good cycling stability (8.4% capacitance decay after 10 000 charge–discharge cycles), and good flexibility (CV curves almost unchanged with different bending angles, Fig. 6d) have also been reported recently.[98] Besides, 3D graphene foams have been used to develop highly deformation-tolerant supercapacitors. In this context, Zhao *et al.*,[56] prepared 3D graphene foam and graphene/polypyrrole composite foam (Fig. 6e–h), through the hydrothermal reduction of aqueous GO dispersions, which can sustain large-strain deformation (*e.g.*, 50% strain) under manual compression and return to the original shape without structural fatigue within 10 s after the stress was released. The CV curves (Fig. 6i) for supercapacitors based on these 3D graphene foams showed no obvious change even after 1000 compression–decompression cycles with a 50% compressed strain.

Recent effort has led to edge-functionalized graphene sheets (EFGs) with various edge groups (*e.g.*, –H, –N, –Br, –Cl, –I, –COOH, –SO_3H) through exfoliation of graphite powders by ball milling.[84,99–102] The unique structure of EFGs with the abundant active sites at the edge and perfect conjugation (conductivity) on the basal plane should lead to high-performance supercapacitors with a high rate capability. The availability of solution-processable EFGs has not only facilitated functionalization of graphene materials but has also allowed the formation of large-area hierarchically-structured graphene films through various solution processing/self-assembling methods which will be useful as electrodes in various energy-related and other devices, such as fuel cells and flexible supercapacitors.[79,84,99–102]

2.3 Free-standing CNT/grapheme hybrid films for flexible supercapacitors

Although the use of 3D graphene foams as electrodes in supercapacitors has been demonstrated to enhance electrochemical performance, there is still a lack of film architecture/property control. One of the attractive options is to use 1D CNTs to physically separate 2D graphene sheets to preserve graphene's high surface area and to provide CNT conducting networks with well-controlled architectures for efficient charge/electrolyte transport.[103–106] Free-standing CNT/graphene composite films for use as electrodes in supercapacitors have been developed by various methods, including layer-by-layer (LBL) self-assembling, vacuum filtration and solution casting.[103–106] By LBL self-assembling poly(ethyleneimine)-modified graphene sheets with acid-oxidized CNTs, for example, Yu and Dai[103] have prepared CNT/graphene hybrid films of interpenetrating network carbon structures with well-defined nanopores which are promising for use in supercapacitor electrodes. The resulting free-standing multilayered

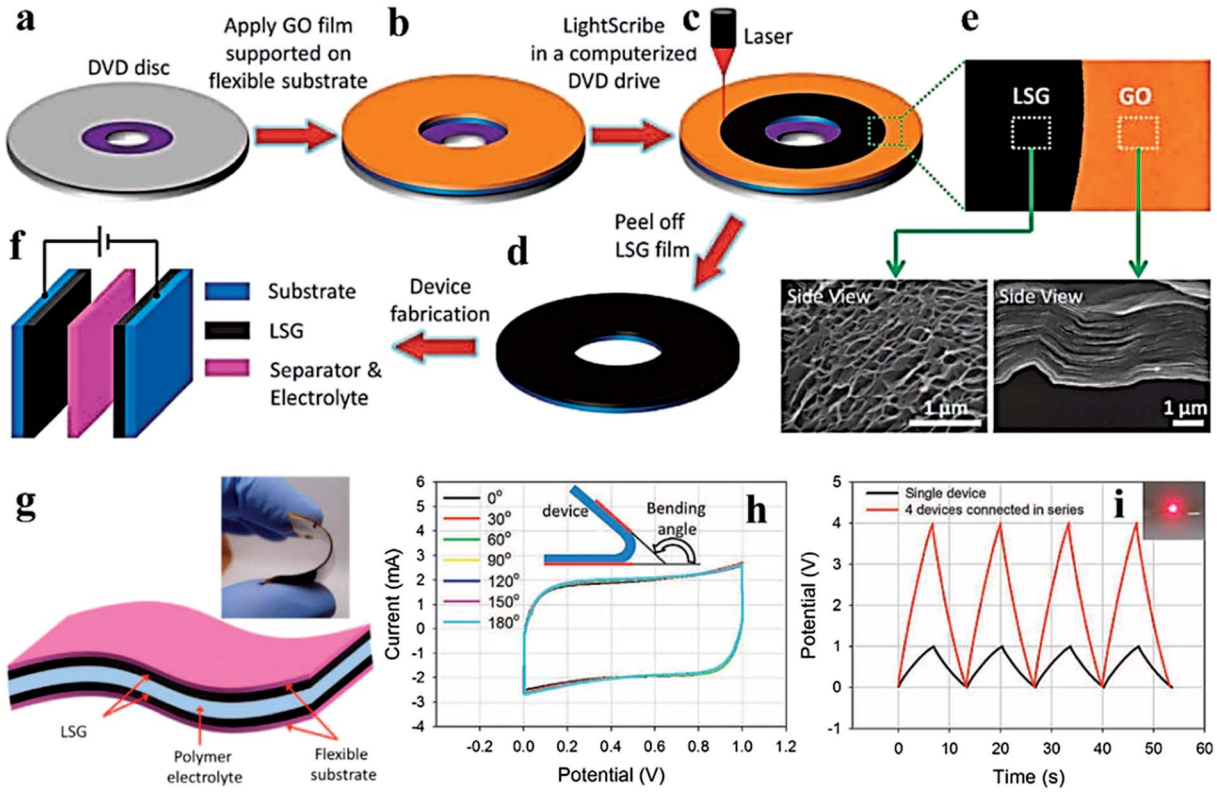

Fig. 5 (a–f) Schematic illustration of the fabrication of laser-scribed graphene-based electrochemical capacitors (EC). (e) Photograph of the GO film changes from a golden brown color to black as it was reduced into laser-scribed graphene. The low-power infrared laser changes the stacked GO sheets immediately into a well-exfoliated few-layered LSG film, as shown in the cross-sectional SEM images. (g) A schematic diagram of the all-solid-state LSG–EC illustrates that the gelled electrolyte can serve as both the electrolyte and separator. The inset is a digital photograph showing the flexibility of the device. (h) CV curves collected at a scan rate of 1000 mV s^{-1} when the device was bent with different angles. (i) Galvanostatic charge–discharge curves for four devices connected in series, the glow of an LED was powered (the inset image).[49] Reproduced from ref. 49 with permission. Copyright 2012, AAAS.

CNT/graphene hybrid film exhibited a nearly rectangular CV even at an exceedingly high scan rate of 1 V s^{-1} with an average specific capacitance of 120 F g^{-1} (three-electrode).

To further improve the electrochemical performance of flexible supercapacitors based on CNT/graphene hybrid electrodes, transition metal oxides have also been introduced into CNT, graphene and their hybrid materials.[104,107] In particular, Cheng *et al.*,[104] have prepared free-standing CNT/MnO_2/graphene composite films with a high MnO_2 loading (71 wt%) and excellent mechanical properties (tensile strength of 48 MPa) through a vacuum filtering method, and demonstrated their use as flexible electrodes in supercapacitors based on liquid electrolytes (*e.g.*, aqueous solution of 1 M Na_2SO_4). Due to the presence of conducting CNT networks in the composite films, a specific capacitance as high as 372 F g^{-1} (three-electrode) with a good rate capability was obtained.

In a somewhat related but independent work, Gao *et al.*,[107] have developed an asymmetric all-solid-state supercapacitor using a free-standing CNT/graphene paper as the negative electrode and a graphene/Mn_3O_4 paper as the positive electrode (Fig. 7a). Both the composite papers were fabricated by filtrating their corresponding mixed solutions. A photograph of the as-prepared CNT/graphene composite paper with a diameter of 4 cm is shown in Fig. 7b while its cross-section SEM image is given in Fig. 7c, which shows the CNTs interposed between the graphene layers. It was found that the specific capacitance of the CNT/graphene paper electrodes increased from 99.7 to 212.9 and 302 F g^{-1} (three-electrode) as the mass ratio of the CNTs increased from 0 to 20% and 40% (Fig. 7d). The total specific capacitance of the asymmetric all-solid-state supercapacitor reached up to 72.6 F g^{-1} (two-electrode) at a current density of 0.5 A g^{-1} with a high energy density (32.7 W h kg^{-1}) and good cycling stability (retained 86.0% of its initial capacitance after 10 000 cycles).

2.4 3D pillared CNT/graphene architectures for flexible supercapacitors

As can be seen from the above discussions, some successes in fabricating randomly oriented CNT/graphene hybrid electrodes for supercapacitors have been recently achieved. However, it is difficult, if not impossible, to control the porosity and hole distribution within the randomly oriented CNT/graphene hybrid materials as each of the constituent CNTs and graphene sheets are randomly assembled together.[51,108–110] Recent theoretical studies[108–112] have indicated that 3D pillared architectures (Fig. 8a),[51] consisting of parallel graphene layers

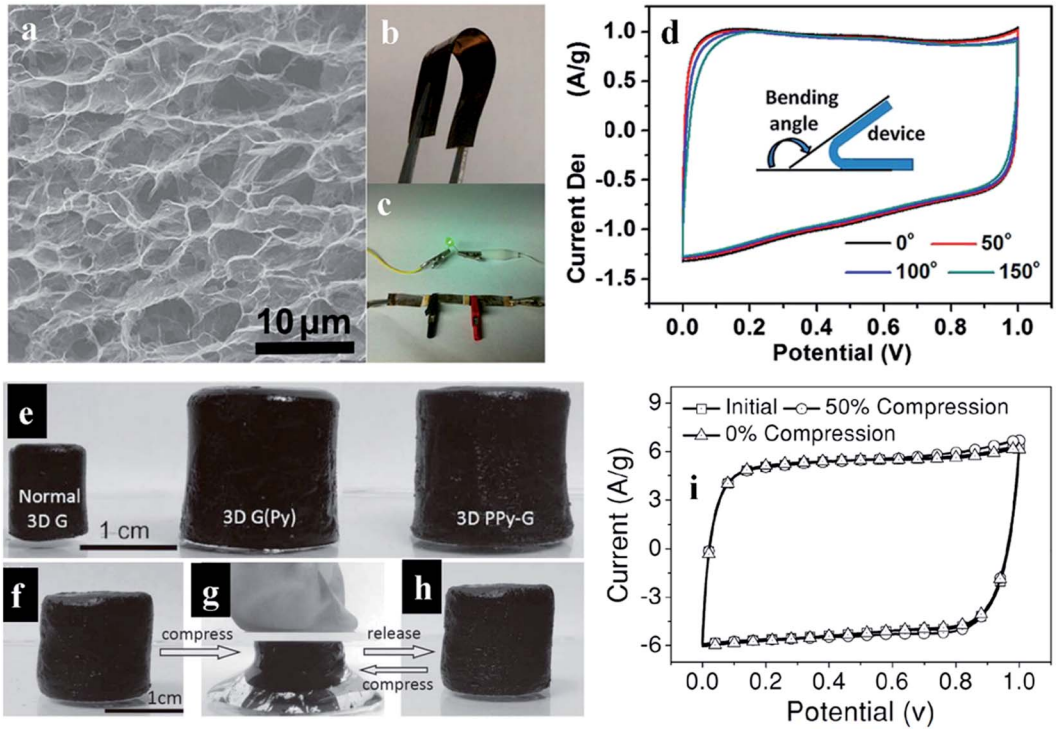

Fig. 6 (a) SEM image of the interior microstructure of a graphene hydrogel. (b) photograph of the flexible solid-state supercapacitor based on the graphene hydrogel film. (c) Photograph of a green LED powered by the three supercapacitors in series. (d) CV curves of the flexible solid-state device at 10 mV s^{-1} for different bending angles.[98] Reproduced from ref. 98 with permission. Copyright 2013. American Chemical Society. (e) Photographs of as-prepared normal 3D graphene, 3D graphene-pyrrole (G-Py) and 3D graphene-polypyrrole (PPy-G) (from left to right). (f–h) The compression–decompression processes of PPy-G foam. (i) CVs of the compressible supercapacitor cells based on the PPy-G foam electrodes under 0% and 50% compression for one cycle at the scan rate of 30 mV s^{-1}.[56] Reproduced from ref. 56 with permission. Copyright 2013, John Wiley and Sons.

supported by VA-CNTs in between, possess a good structural tunability as well as desirable transport and mechanical properties for efficient energy storage.[51] In the 3D pillared structure, VA-CNTs can not only act as mechanical supports for the graphene layers but also provide good conductive paths for efficient electron and ion transport, and hence high capacitance and excellent rate capability. Following theoretical prediction that the 3D pillared CNT/graphene hybrid architecture can be designed with tunable pore sizes and surface areas,[108–110] 3D pillared VA-CNT/graphene architectures with alternating VA-CNTs of different nanotube lengths/packing densities and graphene layers (Fig. 8b) have been prepared by intercalated CVD growth of VA-CNTs into thermally-expanded highly ordered pyrolytic graphite (HOPG).[51] The use of the resultant 3D pillared VA-CNT/graphene hybrids as electrodes in a three-electrode system led to a specific capacitance of about 110 F g^{-1}.[51] After coating with nickel hydroxide, a high specific capacitance of 1065 F g^{-1} (Fig. 8c) with a remarkable rate capability and excellent long-term electrochemical stability (only 4% capacity loss after 20 000 charge–discharge cycles) was achieved. This value is about ten times that of the high-surface-area activated carbons (<100 F g^{-1})[113] and at the same level of 953–1335 F g^{-1} for graphene-supported single-crystalline nickel hydroxide hexagonal nanoplates.[114]

More recently, Lin *et al.*,[115] have reported 3D CNT/graphene-based microsupercapacitors (Fig. 8d–h) fabricated *in situ* on nickel electrodes. A high volumetric energy density of 2.42 mW h cm^{-3} (Fig. 8i) in the ionic liquid was reported, which is higher than that of LSG–DLC,[49] and two orders of magnitude higher than that of aluminum electrolytic capacitors.[116] In addition, the ultrahigh rate capability of 400 V s^{-1} enabled the microdevices to possess a maximum power density of 115 W cm^{-3} in aqueous electrolyte and 135 W cm^{-3} in BMIM–BF4 (Fig. 8j). These results clearly indicate that the 3D pillared CNT/graphene hybrid architectures have ensured high performance for supercapacitors based on liquid electrolytes, in good agreement with theoretical simulations. Therefore, they should also be attractive candidates for use as electrode materials for high-performance flexible all-solid-state supercapacitors, though this is yet to be experimentally realized.

3 Flexible micro-supercapacitors with ultrathin in-plane structures

As can be seen from the above discussions, electrodes based on graphitic carbon nanomaterials were constructed in a typically stacked geometry in supercapacitors with planar structures (Fig. 2). This arrangement often causes insufficient utilization of the carbon-based electrode surface area, and limits

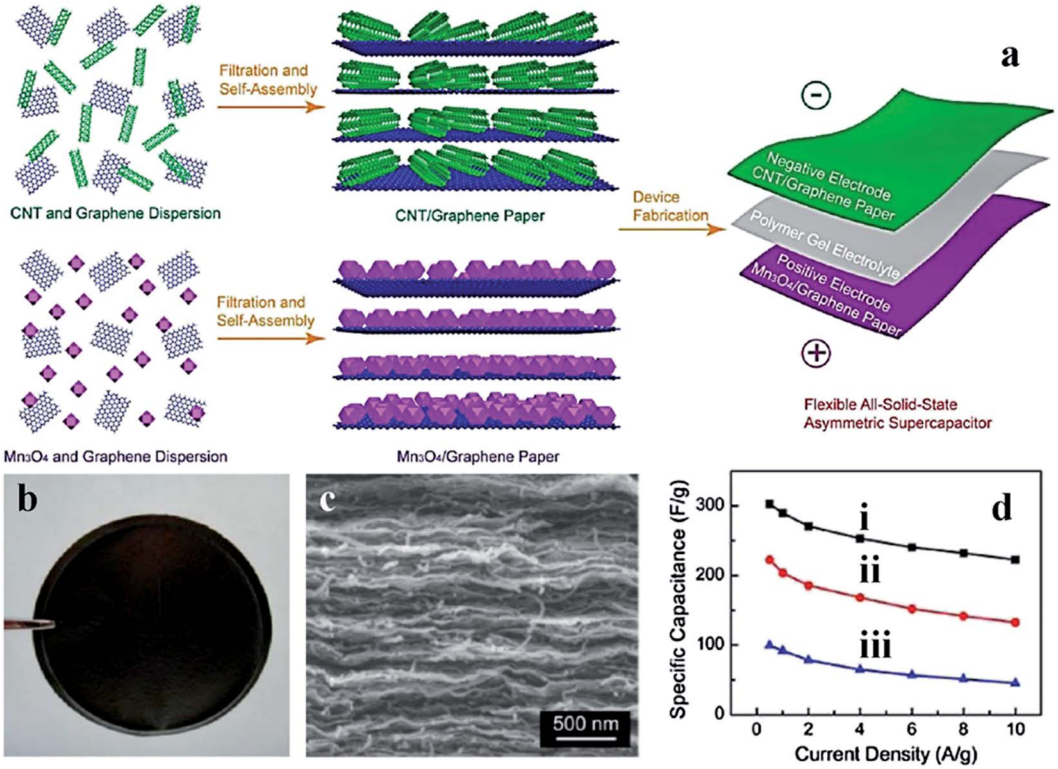

Fig. 7 (a) Illustration of the fabrication process for flexible all-solid-state asymmetric supercapacitors based on free-standing CNT/graphene and Mn_3O_4/graphene paper electrodes. (b) Photograph of CNTG-40 paper with a diameter of 4 cm. (c) Cross-section SEM image of CNTG-40 paper. (d) Specific capacitance of CNTG-40 (i), CNTG-20 (ii), and rGO (iii) papers as a function of discharge current densities. (CNTG-40 and CNTG-20 represent CNT/graphene paper with a CNT mass ratio of 40% and 20%, respectively).[107] Reproduced from ref. 107 with permission. Copyright 2012. American Chemical Society.

electrolyte diffusion into the electrode and the extent of the electrochemical double layers formed at the interface. Thus, supercapacitors with planar structures often show relatively low charge–discharge rates, along with relatively low energy and power densities. Therefore, ultrathin in-plane micro-supercapacitors have been developed to offer ultrahigh power densities that are several orders of magnitude higher than those of conventional supercapacitors and batteries due to their short ion diffusion length.[18,116–118] Various electrode materials, including CNTs,[70] activated carbon,[116] carbide-derived carbons,[18] polymers,[119] and metal oxides,[120] have been investigated for the newly-developed micro-supercapacitors. Due to their excellent in-plane electrical conductivity, large surface area, and easy fabrication (by CVD or reduced from GO), graphene has been widely exploited as an electrode material in micro-supercapacitors.[45,50,118,121] For example, Yoo *et al.*,[50] have developed an in-plane ultrathin supercapacitor (Fig. 9a and b) with electrodes based on pristine graphene and reduced GO multilayers. The open architecture and the effect of graphene edges enabled even the thinnest of devices (made from the as-grown 1–2 graphene layers) to reach specific capacities of up to 80 μF cm^{-2} (Fig. 9c and d), while a much higher (394 μF cm^{-2}) specific capacitance was obtained for the multilayer reduced GO electrodes (with 10 nm thick).

Recently, Wu *et al.*,[45] have developed novel all-solid-state graphene-based in-plane interdigital micro-supercapacitors on both rigid and flexible substrates through micropatterning of graphene films with a nanoscale thickness of 6–100 nm (Fig. 10a–g). The resulting micro-supercapacitors (Fig. 10h and i) delivered an area capacitance of 80.7 μF cm^{-2} (322.8 μF cm^{-2} in electrode) and a stack capacitance of 17.9 F cm^{-3} (71.6 F cm^{-3} in electrode) (Fig. 10j and k). These authors showed a power density of 495 W cm^{-3} (higher than that of electrolytic capacitors), an energy density of 2.5 mW h cm^{-3} (comparable to that of lithium thin-film batteries), and a superior cycling stability. Such microdevices allowed for operations at ultrahigh rates of up to 1000 V s^{-1} (Fig. 10j), three orders of magnitude higher than that of conventional supercapacitors. More importantly, in-plane micro-supercapacitors showed great potential to be integrated into compact on-chip energy storage systems. For instance, El-Kady and Kaner[122] have developed a scalable fabrication process for constructing graphene-based micro-supercapacitors over large areas by direct laser writing on graphite oxide films using a standard LightScribe DVD burner. More than 100 micro-supercapacitors can be produced on a single disc within 30 min or less. These devices can be built on flexible substrates for flexible electronics and on-chip uses, which can be easily integrated with MEMS or CMOS in a single chip. Miniaturized devices at the microscale could enhance the charge-storage

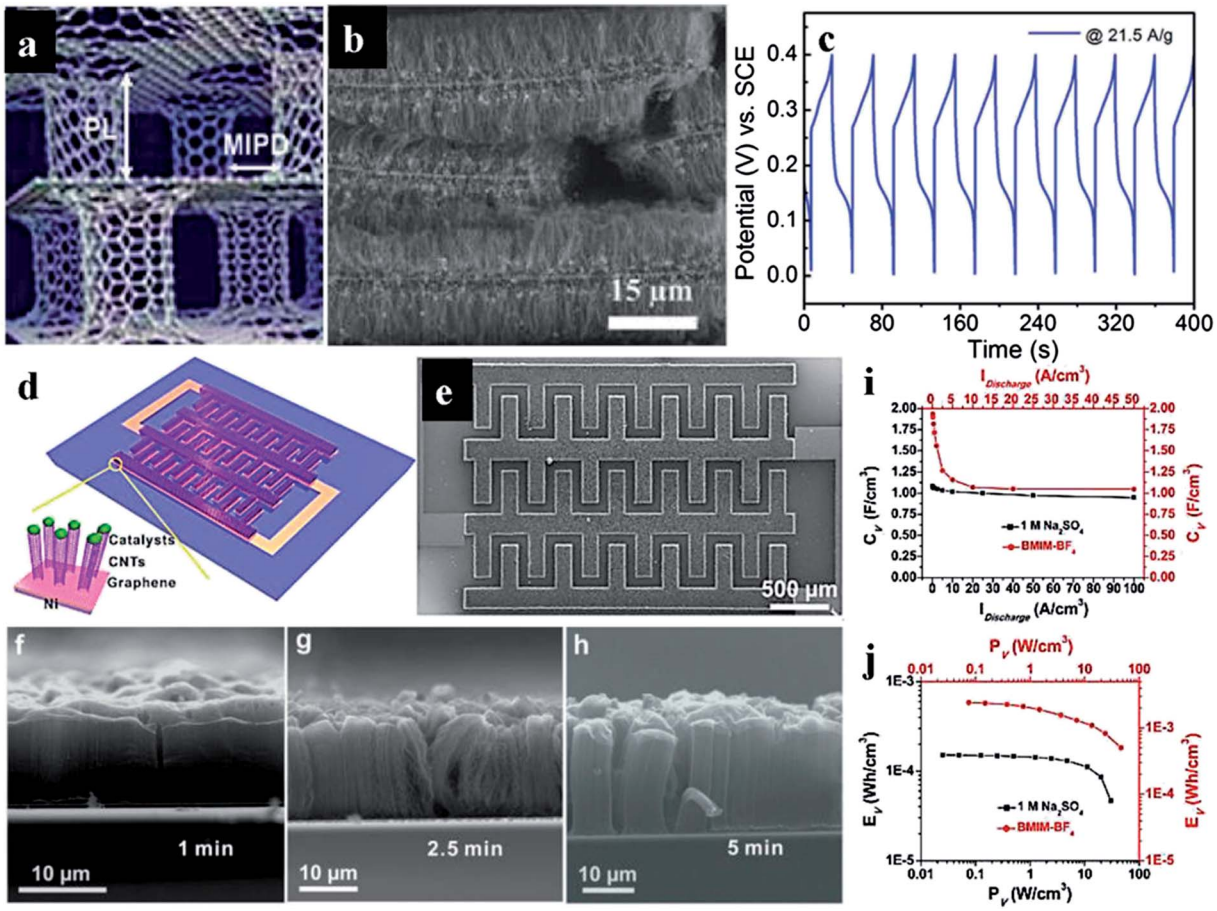

Fig. 8 (a) Schematic diagram of a 3D pillared VA-CNT/graphene nanostructure. (b) Typical SEM image of the 3D pillared VA-CNT/graphene architecture. (c) Galvanostatic charge and discharge curves for the $Ni(OH)_2$-coated VA-CNT/graphene electrode at a current density of 21.5 A g^{-1}.[51] Reproduced from ref. 51 with permission. Copyright 2011. American Chemical Society. (d) Schematic of the structure of G/CNTCs–MCs. Inset: enlarged scheme of Ni–G–CNTCs pillar structure that does not show the Al_2O_3 atop the CNTCs. (e) SEM image of a fabricated G/CNTCs–MC. (f–h) cross-sectioned SEM images of CNTCs grown for 1, 2.5, and 5 min. (i) Comparison of volume specific capacitance (C_V) *versus* discharge volumetric current densities; (j) comparison, in the Ragone plots, of specific volumetric power density (P_V) and energy density (E_V).[115] Reproduced from ref. 115 with permission. Copyright 2013. American Chemical Society.

capacity and rate capability, leading to a power density of 200 W cm^{-3}, the highest value achieved for any supercapacitor to date.[122]

4 Wearable fiber-like supercapacitors based on carbon nanomaterials

As we can see from the above discussions, various supercapacitors with planar structures, including those based on cotton or other textile electrodes decorated with CNTs or graphene, have been developed.[32,58,123,124] However, the rapid development of wearable electronics[125] requires fiber-shaped flexible and wearable supercapacitors. Therefore, wearable fiber-shaped supercapacitors have attracted increasing attention,[46,126–129] and various fiber materials, such as Kevlar fiber[46], metal fiber[126], carbon fiber[127], CNT fibers,[128] and graphene fiber[129], have been exploited as the substrates. Of particular interests, CNT fibers have been extensively studied due to their excellent electrical conductivity, good mechanical properties, and outstanding flexibility.[52,128,130,131] Ren *et al.*,[128] were the first to introduce the CNTs into the fiber-shaped supercapacitors with a twisted structure and relatively low specific capacitance (0.006 mF cm^{-1}). The specific capacitance for one single electrode was then improved to as high as 294 F g^{-1} or 282 mF cm^{-1} by a pseudocapacitive effect generated from conductive PANI hybridized with the CNT fiber.[130]

Recently, Lee *et al.*,[52] used a gradient biscrolling technology to provide a fast-ion-transport yarn (Fig. 11a), in which hundreds of multiwalled CNT (MWCNT) layers infiltrated with conductive polymer (*e.g.*, poly(3,4-ethylenedioxythiophene)) were scrolled into a yarn of about 20 μm thickness. A metal wire was used as the current collector to increase power generation by plying with the biscrolled yarn (Fig. 11b). The discharge current of the plied yarn supercapacitor increased linearly with the voltage scan rate up to 80 V s^{-1} and 20 V s^{-1} for liquid and solid electrolytes, respectively. The resultant fiber-shaped supercapacitors exhibited a high stability; the capacitance changed a little when the capacitor was bent (~2% for 2000

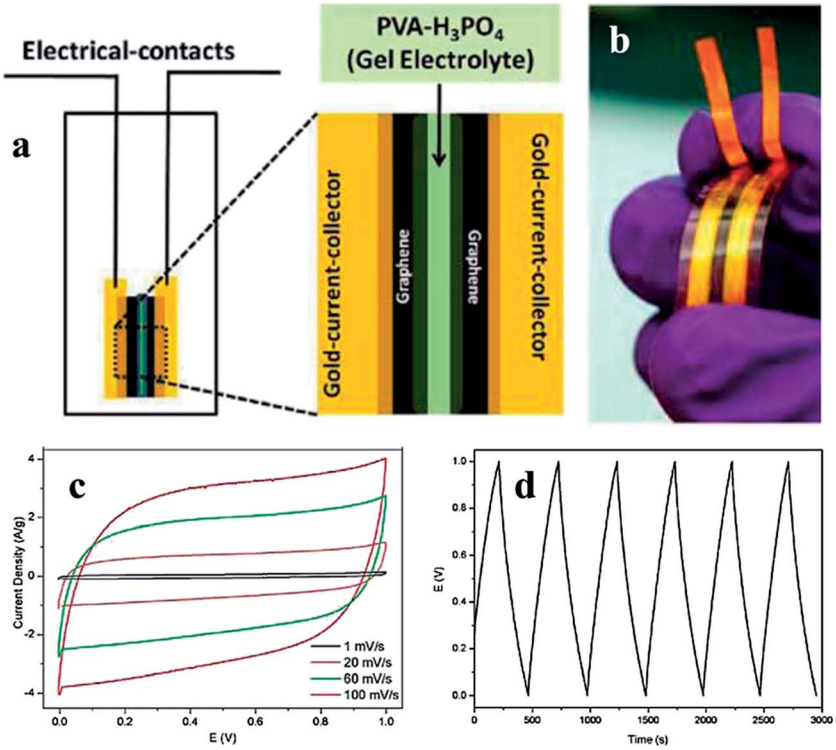

Fig. 9 (a) Schematic depiction of the device fabricated using the concept of 2D in-plane supercapacitors (b) A prototype flexible supercapacitor device based on reduced multilayer GO (RMGO) developed using the new in-plane geometry. (c) CV curves obtained at different scan rates for RMGO. (d) Galvanostatic charge–discharge curve of the RMGO supercapacitor measured at constant current density of 176 mA g^{-1}.[50] Reproduced from ref. 50 with permission. Copyright 2011. American Chemical Society.

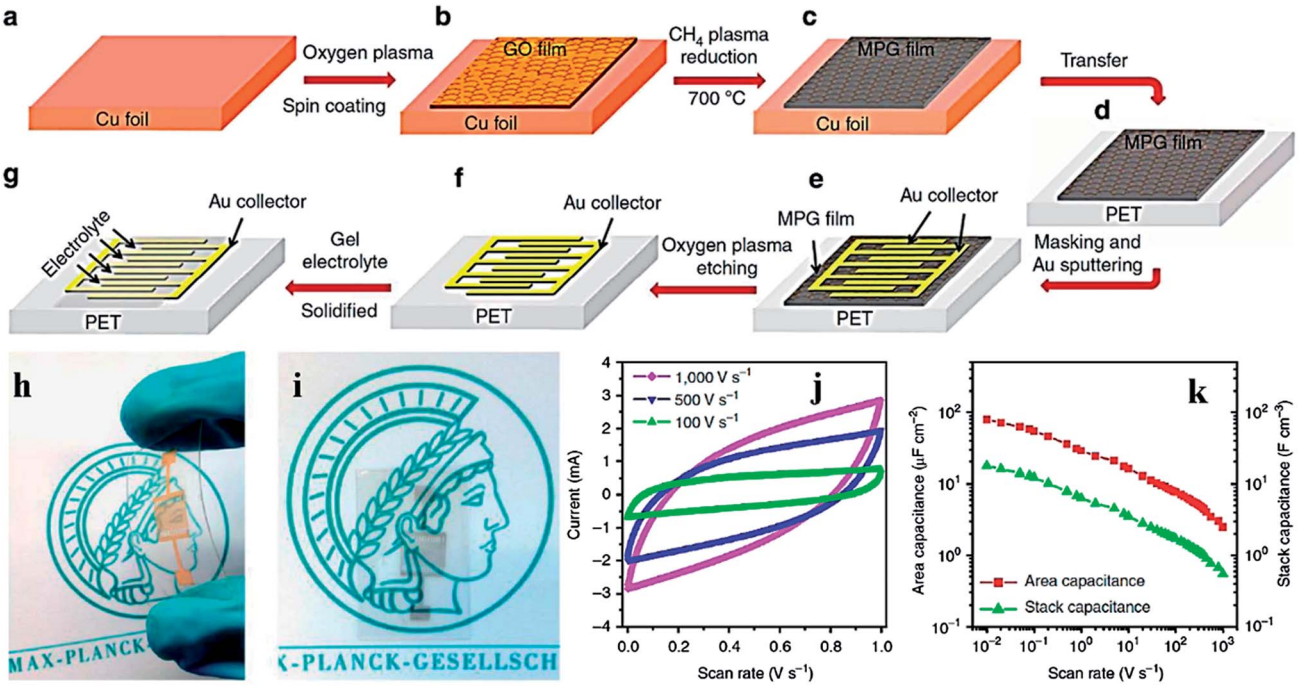

Fig. 10 (a–g) Schematic illustration of the fabrication of flexible MPG–MSCs–PET. (h and i) The resulting MPG–MSCs–PET (h) with and (i) without Au collectors, showing the flexible and transparent characteristics of the fabricated microdevices. (j) CV curves of the MPG–MSCs–PET obtained at different scan rates of 100, 500 and 1000 V s^{-1} with a typical electric double-layer capacitive behavior even at ultrahigh scan rates, demonstrating its ultrahigh power ability. (k) Area capacitance and stack capacitance of the MPG–MSCs–PET.[45] Reproduced from ref. 45 with permission. Copyright 2013, Nature Publishing Group.

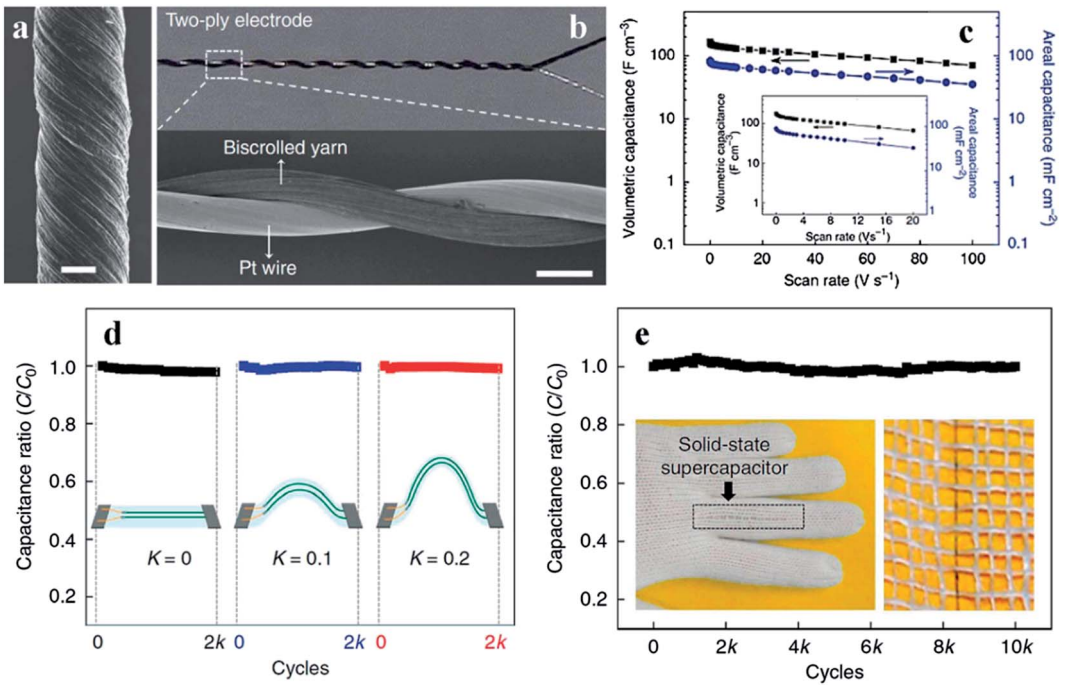

Fig. 11 (a) SEM images of a biscrolled yarn with ~37° bias angle. Scale bar, 10 μm. (b) Two SEM images of a PEDOT/MWCNT biscrolled yarn that is plied with a 25 μm Pt wire. Scale bar, 40 μm. (c) Volumetric capacitance *vs.* scan rate. (d) Bending on a flexible polyethylene terephthalate film (*k* is curvature in mm^{-1}). (e) Weaving into a glove (the yarn supercapacitor was 5 cm long).[52] Reprinted from ref. 52 with permission. Copyright 2013, Nature Publishing Group.

cycles, Fig. 11d) or woven into a glove (~1% for 10 000 cycles, Fig. 11e).

5 Stretchable supercapacitors based on carbon nanomaterials

Stretchable electronics with highly stable performance under strain have recently attracted a great deal of interest. Stretchable electronics,[132] including transistors,[133] polymer light-emitting diodes,[134] polymer solar cells,[135] and active matrix displays,[136] have been developed to maintain their electronic performance even under large levels of mechanical deformation (up to 40% strain). Highly stretchable electronics have opened up exciting opportunities for the development of large-area, light-weight, and wearable electronics. Like other stretchable optoelectronic units (*e.g.*, organic solar cells, light-emitting diodes, and field effect transistors), stretchable supercapacitors are critical components in power-integrated flexible optoelectronic systems.[47,137–139] Buckled single-walled carbon nanotube (SWCNT) macrofilm electrodes, generated by coating a thin SWCNT film onto a pre-strained elastomeric substrate (PDMS) and followed by stress releasing, were among the first stretchable electrodes used for supercapacitors. The electrochemical performance of supercapacitors based on these buckled SWCNTs remained almost unchanged under stretching with 30% strain.[47] Recently, Niu *et al.*,[138] have developed highly stretchable buckled SWCNT films (Fig. 12a–c) by directly growing SWCNT films with reticulate architecture on a PDMS substrate with enhanced pre-strain, the electrical resistance of the resultant electrode had no significant change even under a high strain of 140%. All-solid-state stretchable supercapacitors were developed by using H_2SO_4–PVA gel as both the electrolyte and the separator, which can also efficiently overcome separation of the two electrodes under strain (Fig. 12d–g). The resulting supercapacitors exhibited high stretchability with no obvious difference at low potentials and only very small deviation at higher potentials in their CV curves (Fig. 12h) upon stretching up to 120% strain. The charge–discharge performance was also very stable even under 120% strain (Fig. 12i), from which specific capacitances of 48 and 53 F g^{-1} were obtained for the supercapacitor without and with applied 120% strain. In order to take combined advantage of the high conductivity and flexibility of CNTs and high pseudo-capacitance of conductive polymers, CNT and conductive polymer (*e.g.*, polypyrrole) composites have also been exploited in stretchable supercapacitors with the capacitance reduced by 5.6% at 30% strain.[140]

Unlike stretchable supercapacitors with planar structures, it is a big challenge to construct fiber-shaped stretchable devices because most fiber substrates are neither stretchable nor conductive and some of them are either stretchable but of low conductivity (*e.g.*, elastic polymer fibers) or conductive but of low stretchability (*e.g.*, metal wires). A great breakthrough has been made recently by Peng's group.[53] These authors have developed stretchable coaxial fiber-shaped supercapacitors by using an elastic fiber wrapped with aligned CNT sheets with a polymer gel sandwiched between the two coaxial CNT layers as the electrolyte and separator. The resultant fiber-shaped

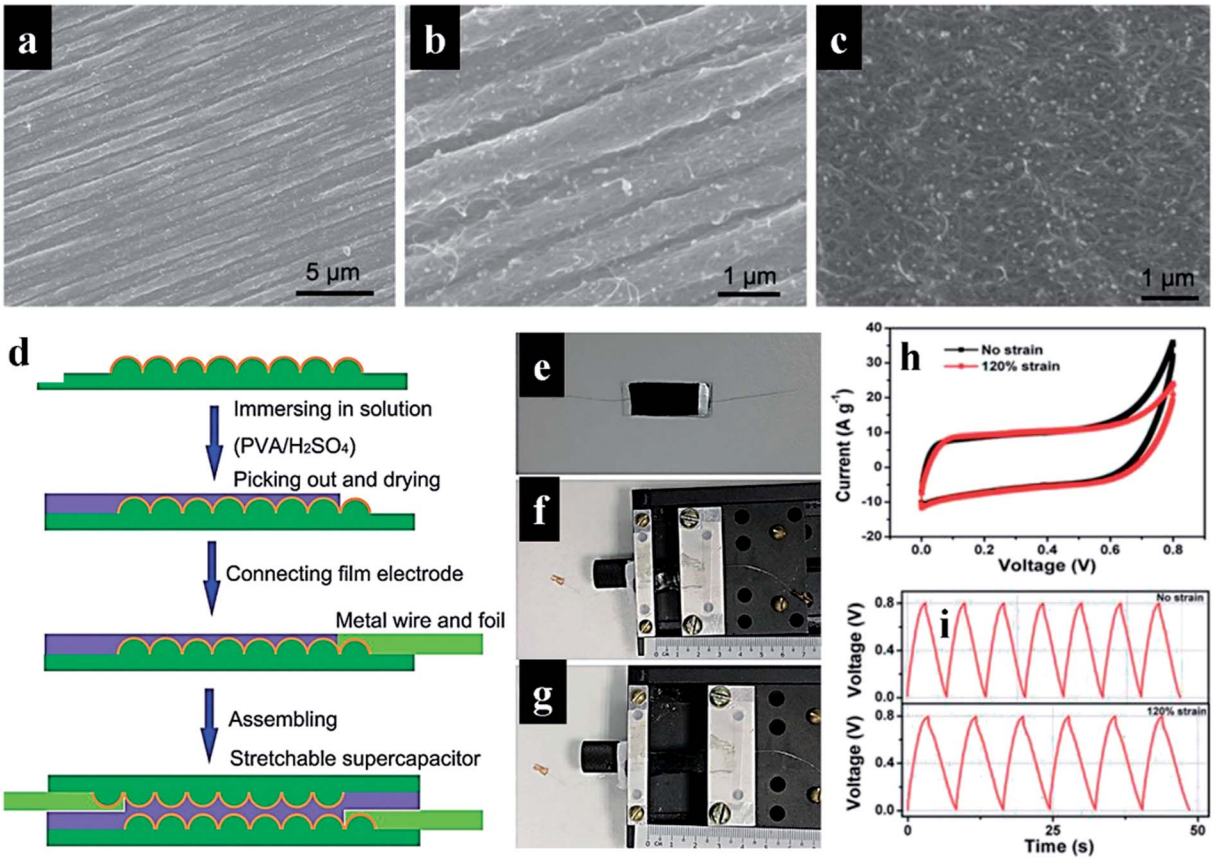

Fig. 12 (a–c) SEM images of buckled SWCNT film without strain at low (a), high (b) magnifications and with 100% strain (c). (d) Schematic of preparation of integrated stretchable supercapacitors based on buckled SWCNT films on PDMS. (e) The optical image of an integrated stretchable supercapacitor based on buckled SWCNT films on PDMS. (f and g) Optical images of a stretchable supercapacitor without strain (f) and with about 120% strain (g). (h) CV curves of a representative stretchable supercapacitor with and without 120% strain at a scan rate of 200 mV s^{-1}. (i) The galvanostatic charge–discharge curves of the stretchable supercapacitor with and without 120% strain at a constant current of 10 A g^{-1}.[138] Reproduced from ref. 138 with permission. Copyright 2013, John Wiley and Sons.

supercapacitor exhibited a high stretchability and stability; its CV curve (Fig. 13b) remained unchanged even under 75% strain while its specific capacitance was maintained by more than 95% over 100 stretching cycles with a strain of up to 75% without any obvious structural damage (Fig. 13c).

6 Transparent and stretchable supercapacitor based on carbon nanomaterials

Apart from flexible/stretchable supercapacitors, transparent energy conversion (*e.g.*, solar cells,[141,142] OLEDs[143]) and storage (*e.g.*, batteries,[144] supercapacitors[145–147]) devices are a recent development, which show great promise as power sources for automobile/building windows or personal electronics with high aesthetic appeal. Some transparent supercapacitors based on carbon film (*e.g.*, CNTs, graphene) have recently been reported.[145–147] However, it remains a big challenge to develop supercapacitors with both good optical transmittance and mechanical stretchability because most of the existing electrodes are either transparent but rigid (*e.g.*, ITO, other metal oxides), or stretchable but opaque (*e.g.*, conducting polymer films), or neither transparent nor stretchable (*e.g.*, metal electrodes). By directly drawing CNT thin films from VA-CNT arrays onto transparent and stretchable substrates (*e.g.*, PDMS), Chen *et al.*, developed the first CNT-based electrodes with a high transmittance (as high as 78% at the wavelength of 550 nm) and stretchability, which, after coating with a layer of PVA–H_3PO_4 electrolyte, showed only 80% increase in electrical resistance under 30% strain.[35] Subsequently, these authors developed transparent and stretchable all-solid-state supercapacitors (Fig. 14a and b) by directly pressing two of the PDMS-supported CNT electrodes with the PVA–H_3PO_4 gel electrolyte, which also acted as the separator, sandwiched in between.[35] The device based on the electrodes with one single layer CNT sheet in a cross assembled configuration (Fig. 14b) showed a transmittance of 75% (Fig. 14c), comparable to that of a pure single layer CNT sheet supported by PDMS. Nevertheless, the corresponding device with a parallel assembled configuration (Fig. 14a) had a transmittance of 64%, presumably due to the extensive overlap of CNTs between the two parallel electrodes. The cross assembled device exhibited a good stretchability in biaxial directions, and its specific capacitance was almost

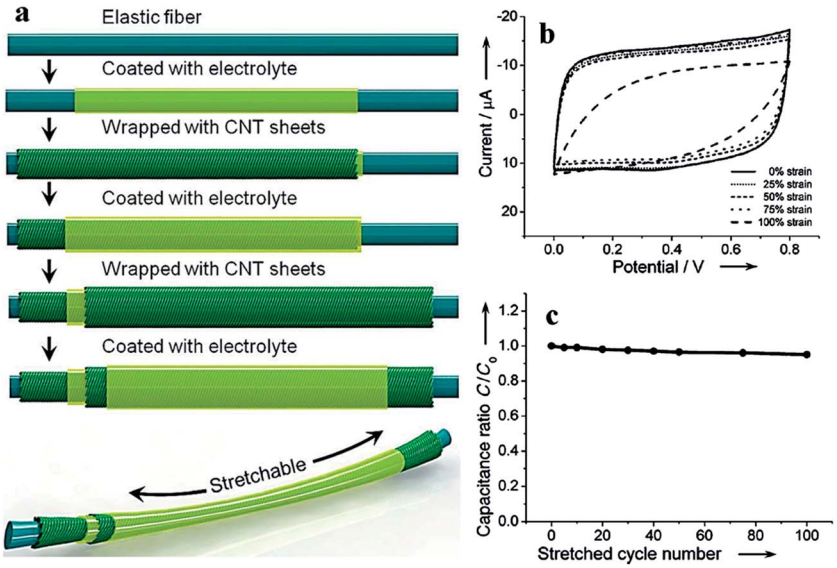

Fig. 13 (a) Illustration of the fabrication of a highly stretchable, fiber-shaped supercapacitor with a coaxial structure. (b) CV curves of the fiber-shaped supercapacitor with increasing strains from 0 to 100%. (c) Dependence of specific capacitance on stretched cycle number with a strain of 75%.[53] Reproduced from ref. 53 with permission. Copyright 2013, John Wiley and Sons.

unchanged even up to 30% strain (Fig. 14d). The cross assembled supercapacitor was also shown to have better stability than that of its parallel counterpart (Fig. 14e). For comparison, the parallell assembled supercapacitor showed an over 70% increase in capacitance during the initial twenty stretching cycles before reaching to a stable capacitance. This capacitance increase with the stretching cycles could be attributed to the combined effects associated with the stretching-induced increase in the active sites of the CNT sheet and loss of the nanotube–nanotube contacts.[35] Both types of supercapacitors were shown to have good stability even after hundreds of stretching cycles, exhibiting great potential for practical applications.

Along with the development of transparent CNT electrodes, graphene has also been used for the same application due to its excellent optical and electrical properties.[148–150] Although some

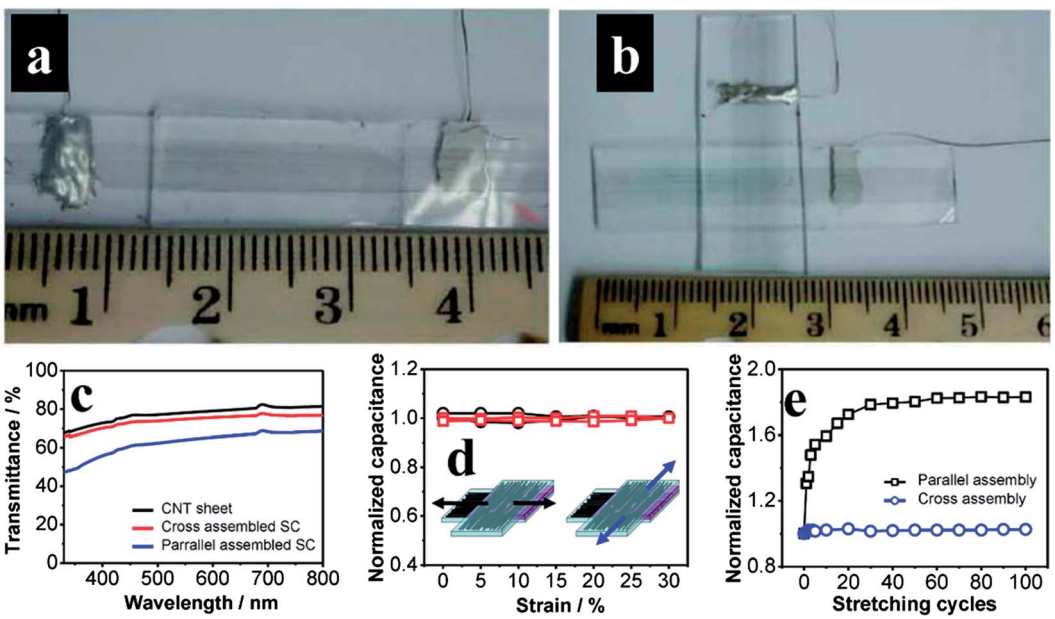

Fig. 14 (a and b) Photographs of supercapacitors assembled in the parallel and cross configurations. (c) Transmittance spectra of a single layer CNT sheet on the PDMS substrate and the associated supercapacitors with parallel and cross configurations. (d) Normalized specific capacitance of the supercapacitor with cross assembly as a function of the tensile strain as it was biaxially stretched. (e) Normalized specific capacitance of the two type supercapacitors as a function of stretching cycles.[35] Reprinted from ref. 35 with permission. Copyright 2014, Nature Publishing Group.

graphene-based stretchable electrodes and electronic devices have been reported,[147,148] their performance is still largely limited by the easy damage of the graphene sheet upon stretching. For instance, the electrical resistance of a graphene sheet transferred onto a pre-strained elastic substrate increased by more than one order upon 25% strain.[148] Besides, it is difficult to transfer as-grown graphene with an area of up to 2 × 2 cm^2 to a pre-strained substrate because cracking or breaking of the graphene sheet often occurs during the transferring process. As such, very limited effort has been made to develop transparent and stretchable graphene electrodes, as it is very difficult, if not impossible. Owing to its high conductivity and excellent transparency (transmittance up to 95% for 2 nm thick film[81]), however, the one-atom-thick and/or few-layered graphene sheets provide ideal electrode materials for high-performance stretchable and transparent optoelectronics. In order to realize this possibility, Chen *et al.*,[55] have designed and synthesized the first wrinkled few-layered graphene sheet (Fig. 15a), from which transparent and stretchable all-solid-state supercapacitors (Fig. 15b and c) have been developed. Due to its unique structure, the PVA/H_3PO_4-coated wrinkled multilayered graphene sheet on a PDMS substrate was shown to be highly stretchable and the electrical resistance increased by only 170% under 40% strain (Fig. 15d),[55] which is better than any stretchable planar graphene electrode previously reported.[148] The resulting wrinkled graphene not only had good stretchability, but also showed a high transmittance of ~60% at 550 nm. The transmittance for supercapacitors based on the wrinkled graphene electrodes also reached up to 57% (Fig. 15e) with no obvious changes in the electrochemical performance upon stretching up to 40% strain (Fig. 15f), and no serious structural damage after 100 stretching cycles with strain from 0% to 40% (Fig. 15g).

The above results show the good optical transparency and mechanical stretchability of supercapacitors based on wrinkled graphene electrodes which will be useful for various applications, ranging from portable energy sources for flexible electronics to energy storage components in various stretchable integrated systems. It is worth noting that the performance of these newly-developed transparent and stretchable supercapacitors based on wrinkled graphene electrodes is still limited by the low specific surface area of the horizontally stacked graphene sheets and the absence of a metal current collector. Therefore, there is still considerable room for future improvement of the device performance for stretchable and transparent supercapacitors through optimization of the electrode/device structure, for example by incorporating conductive polymers and/or metal oxides into the carbon electrode nanomaterials.

7 Integration of flexible supercapacitors with other energy devices

Traditionally, external conductive wires are required to store the electric energy from an energy conversion device (*e.g.*, solar cell) into an energy storage device (*e.g.*, supercapacitor or battery). To reduce/eliminate the unnecessary energy loss inevitably associated with external conductive wires, self-powering systems integrated with energy conversion and storage devices to realize simultaneous energy conversion and storage in a single device

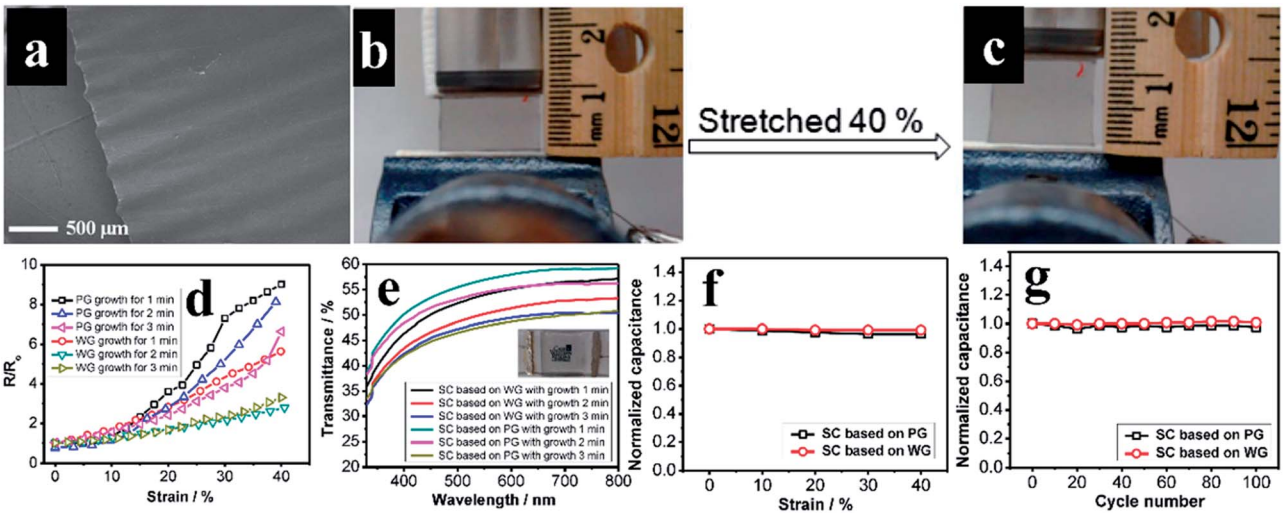

Fig. 15 (a) Typical SEM image of the as-synthesized wrinkled graphene sheet on a PDMS substrate from the top view. (b and c) Digital photographs of the supercapacitors before (b) and after (c) being stretched up to 40% strain. (d) Dependency of resistance of the PVA-coated planar and wrinkled graphene sheets with different CVD deposition times on the tensile strain. (e) Transmittance of supercapacitors (SC) based on the planar graphene (PG) and wrinkled graphene (WG) sheets with different CVD deposition times. The inset of (e) shows a digital photograph of a supercapacitor device on a piece of paper printed with Case logo to demonstrate its transparency. (f) Normalized surface-specific capacitance of the supercapacitors based on either the planar or wrinkled graphene sheet as a function of tensile strains. (g) Normalized surface-specific capacitance of supercapacitors based on either the planar or wrinkled graphene sheet as a function of stretching cycles.[55] Reproduced from ref. 55 with permission. Copyright 2014. American Chemical Society.

have been recently developed.[151–154] Due to their excellent optical and mechanical properties, carbon nanomaterials (*e.g.*, CNTs, graphene) have also been used in the integrated systems, either flexible or non-flexible, as efficient electrode materials for both energy conversion and storage devices.[48,155] Using a SWCNT network as the integration platform (Fig. 16a and b), for instance, Wee *et al.*,[48] have developed a printable all-solid integrated device consisting of a polymer solar cell (PSC) and a supercapacitor, in which the supercapacitor was charged up by exposing the polymer solar cell under an illumination of 100 mW cm^{-2} (so-called photocharge), and the discharge of the supercapacitor was performed by connecting a resistor as a load after the light source was switched off (Fig. 16a and b). Fig. 16c and d show the voltage and current profiles of the integrated system *vs.* time during the charging and discharging process, from which a capacitance of 28 F g^{-1} can be obtained. An integrated device consisting of an all-solid-state dye-sensitized solar cell and a supercapacitor based on CNT/polyaniline composite electrodes has also been reported (Fig. 16e).[155] From Fig. 16f, it was estimated that the photocharge time was 33 s, galvanostatic discharge time was 144 s, and the entire photoelectric conversion and storage efficiency was 4.29% by multiplying the energy conversion efficiency of the solar cell and the energy storage efficiency of the supercapacitor. Using ITO-coated polyethylene naphthalate as the conductive substrate, Yang *et al.*,[155] have recently developed a flexible integrated device (Fig. 16g), which had a relatively long photocharge time of 183 s (Fig. 16h) with respect to the device prepared on ITO glass (33 s) due to the relatively low photocurrent generated by the flexible solar cell in the flexible integrated system.

For applications in wearable electronics, it is essential to develop integrated devices containing an energy conversion unit and a supercapacitor in a single wire.[54,151,156,157] In this regard, Bae *et al.*,[156] integrated, for the first time, a nanogenerator (for mechanical energy harvesting), a solar cell, and a supercapacitor on a single wire, as schematically shown in Fig. 17a. These authors used the radially grown ZnO nanowires as the active unit for the nanogenerator, the core of the solar cell, and the large-surface-area electrode for the supercapacitor. Conductive and transparent graphene on copper mesh was used as the cylindrical top electrode for each of the integrated energy devices. A Schottky contact was formed at the interface between the graphene and ZnO nanowires (Fig. 17b). Fig. 17c shows the current density–voltage curve for the solar cell unit and an energy conversion efficiency of 0.02% was obtained. The relative low efficiency of the solar cell was attributed to the graphene on copper mesh that was not fully transparent, causing insufficient light absorption. Fig. 17d shows the CV curve for the supercapacitor unit, which has a specific capacitance of 0.4 mF cm^{-2}. The poor performance of the single wire integrated system may be attributable to the mismatch between the two electrodes in use for different energy devices along the wire.

Recently, Chen *et al.*,[54] reported a high-performance fiber-shaped integrated energy wire, consisting of a dye-sensitized solar cell and a supercapacitor (Fig. 17e–g). In this case, radially grown titania nanotubes on a titanium wire were used as the core electrode for both the solar cell and supercapacitor while an aligned CNT fiber was wrapped around the titanium wire, after coating with electrolytes, as the top electrode for the solar

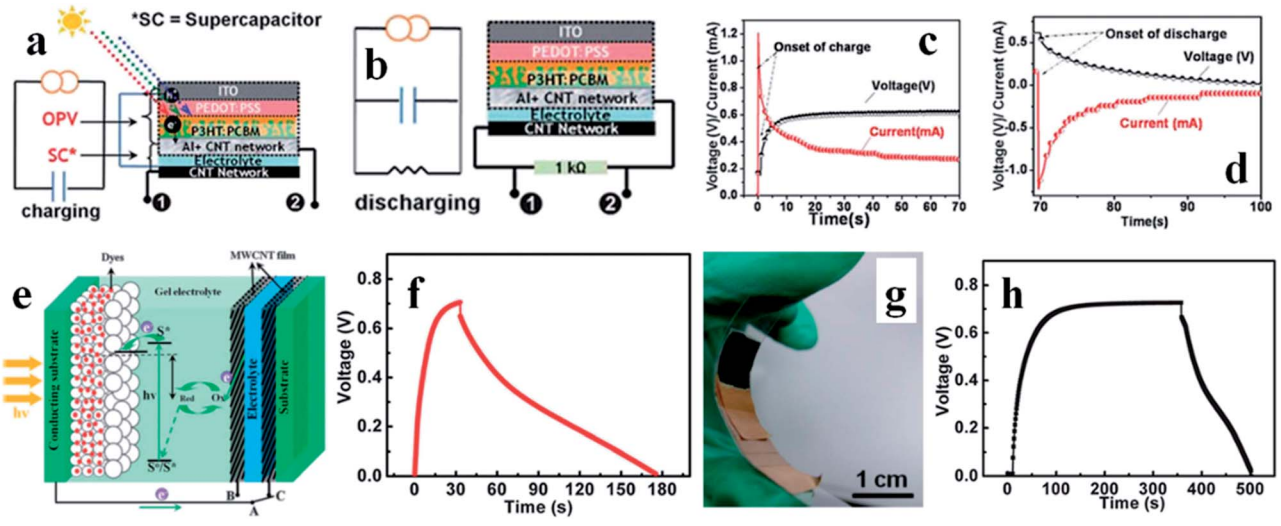

Fig. 16 (a and b) Schematic and equivalent circuit illustration for a PSC during the charging process (a) and galvanostatic discharge (b). (c and d) The voltage and current profiles *versus* time for the charging (c) and discharging (d) process.[48] Reprinted from ref. 48 with permission. Copyright 2011, The Royal Society of Chemistry. (e) Schematic illustration of the integrated device of photoelectric conversion and energy storage based on aligned MWCNT films as electrodes. (f) The dynamic voltage of the device with CNT/PANI composite films as electrodes during photocharging and galvanostatic discharging processes. The photocharge was performed under AM1.5 illumination and discharge was carried out at a constant current density of 1.4 mA cm^{-2}. (g) Photograph of a flexible integrated device during bending. (h) The dynamic voltage during photocharge and galvanostatic discharge processes. The constant discharge current density was 1.4 mA cm^{-2}.[155] Reprinted from ref. 155 with permission. Copyright 2013, The Royal Society of Chemistry.

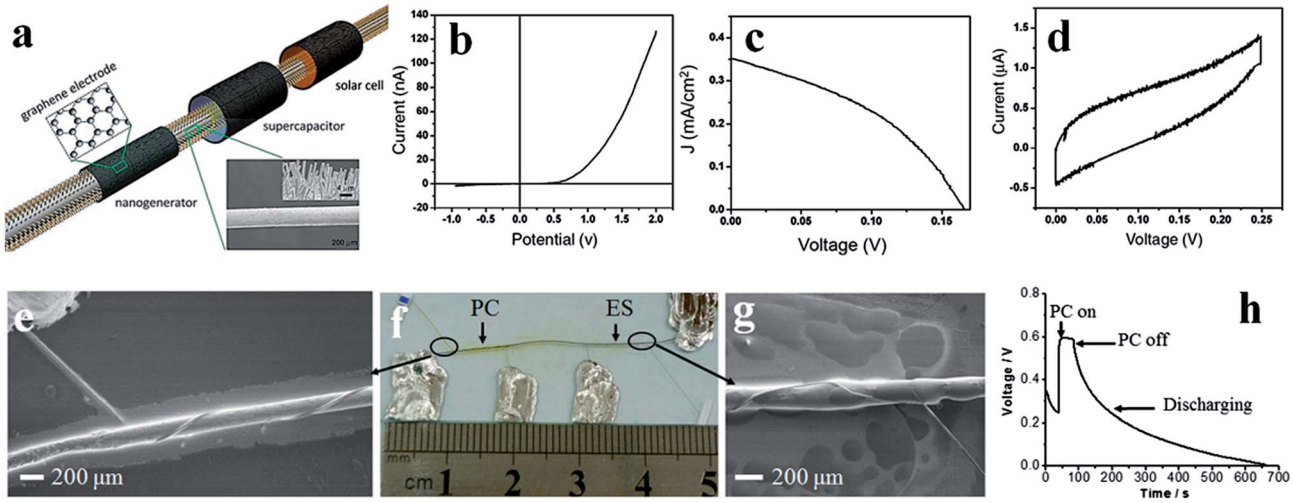

Fig. 17 (a) Schematic of a fiber-based multi-energy device comprising of a nanogenerator (for mechanical energy harvesting), a solar cell (for solar energy harvesting) and a supercapacitor (for electrochemical charge storage). ZnO nanowires (inset SEM image) were grown on a flexible thin plastic wire coated with thin Au film. (b) Current–voltage plot showing the Schottky contact between the ZnO nanowires and graphene top electrode. (c) *J*–*V* curves of the DSSC under one full-sun illumination. The illumination is normal to the plastic wire. (d) Typical cyclic voltammetry of the supercapacitor using PVA/H_3PO_4 as electrolyte at 100 mV s^{-1}.[156] Reproduced from ref. 156 with permission. Copyright 2011, John Wiley and Sons. (e) SEM image of the fiber-shaped integrated energy wire, consisting of photoelectric conversion (PC) and energy storage, at the PC end. (f) Photograph of the entire integrated wire-shaped device. (g) SEM image of the ES at the ES end. (h) Photocharging–discharging curve of the fiber-shaped integrated energy wire. The discharging current is 0.1 μA.[54] Reproduced from ref. 54 with permission. Copyright 2012, John Wiley and Sons.

cell (Fig. 17f and e) and supercapacitor (Fig. 17g). As seen in Fig. 17h, the supercapacitor in this integrated device was rapidly charged up to a voltage close to the open-circuit voltage of the DSSC upon light irradiation. An entire energy conversion and storage efficiency of up to 1.5% was obtained. An integrated power fiber containing a polymer solar cell and a supercapacitor based on carbon nanotubes has also been developed, which represented a truly flexible and wearable fiber-shaped self-powering system of practical significance for portable and wearable electronic applications.[158] Clearly, promising potential for future research exists in this area.

8 Conclusions

Electrochemical supercapacitors represent one of the major emerging energy storage devices due to their long cycling stability and high power densities. Compared with their conventional counterparts, flexible, stretchable and wearable supercapacitors are needed for various emerging applications, ranging from flexible electronics to wearable displays. The synthesis of electrode materials with desirable electrical/mechanical properties and microfabrication of them into devices with required features are key prerequisites for many of the speciality applications. Nanotechnology has opened up new frontiers in materials science and engineering by creating new nanomaterials and technologies for the development of flexible supercapacitors. In particular, carbon nanomaterials, including CNTs and graphene, have been extensively investigated as electrode materials for flexible supercapacitors due to their large surface area, excellent mechanical, optical, electrical and electrochemical properties. As a result, a large variety of flexible, stretchable, wearable and even transparent supercapacitors based on nanocarbon electrodes of different shapes (*e.g.*, planar, fiber-like) with controllable architectures (*e.g.*, aligned, pillared, foam-like) have been developed. The integration of flexible supercapacitors with other energy devices (*e.g.*, solar cells, nanogenerators) into planar and wire-shaped self-powered systems has also been demonstrated. In many cases, however, the material properties and/or device characteristics need to be optimized for further enhancement of the device performance. Recent developments in the field as reviewed in this article have clearly indicated the versatility of carbon nanomaterials for making flexible supercapacitors with novel features for a wide range of specific applications. As far as the published work is concerned, tremendous progress has been made within recent years. There remains, however, much work to do. Continued effort in this promising area could make flexible supercapacitors one of the most powerful and efficient energy storage technologies, which will affect every aspect of our modern society.

Acknowledgements

The authors are grateful for financial support from AFOSR (FA9550-12-1-0037, FA-9550-12-1-0069), NSF (CMMI-1266295, AIR- IIP-1343270, DMR-1106160), DOD-Army (W911NF-11-1-0209) and DAGSI.

Notes and references

1 J. R. Miller and P. Simon, *Science*, 2008, **321**, 651–652.
2 P. Simon and Y. Gogotsi, *Nat. Mater.*, 2008, **7**, 845–854.

3 M. Winter and R. J. Brodd, *Chem. Rev.*, 2004, **104**, 4245–4270.
4 J. Zhang and X. Zhao, *ChemSusChem*, 2012, **5**, 818–841.
5 T. Chen and L. Dai, *Mater. Today*, 2013, **16**, 272–280.
6 J. Gamby, P. Taberna, P. Simon, J. Fauvarque and M. Chesneau, *J. Power Sources*, 2001, **101**, 109–116.
7 E. Frackowiak and F. Beguin, *Carbon*, 2001, **39**, 937–950.
8 L.-F. Chen, Z.-H. Huang, H.-W. Liang, W.-T. Yao, Z.-Y. Yu and S.-H. Yu, *Energy Environ. Sci.*, 2013, **6**, 3331–3338.
9 X. Tao, X. Zhang, L. Zhang, J. Cheng, F. Liu, J. Luo, Z. Luo and H. J. Geise, *Carbon*, 2006, **44**, 1425–1428.
10 J. Huang, B. G. Sumpter and V. Meunier, *Angew. Chem., Int. Ed.*, 2008, **47**, 520–524.
11 D.-W. Wang, F. Li, Z.-G. Chen, G. Q. Lu and H.-M. Cheng, *Chem. Mater.*, 2008, **20**, 7195–7200.
12 D. N. Futaba, K. Hata, T. Yamada, T. Hiraoka, Y. Hayamizu, Y. Kakudate, O. Tanaike, H. Hatori, M. Yumura and S. Iijima, *Nat. Mater.*, 2006, **5**, 987–994.
13 L. Dai, D. W. Chang, J. B. Baek and W. Lu, *Small*, 2012, **8**, 1130–1166.
14 Y. Wang, Z. Shi, Y. Huang, Y. Ma, C. Wang, M. Chen and Y. Chen, *J. Phys. Chem. C*, 2009, **113**, 13103–13107.
15 L. L. Zhang, R. Zhou and X. Zhao, *J. Mater. Chem.*, 2010, **20**, 5983–5992.
16 J. Hou, Y. Shao, M. W. Ellis, R. B. Moore and B. Yi, *Phys. Chem. Chem. Phys.*, 2011, **13**, 15384–15402.
17 J. Chmiola, G. Yushin, Y. Gogotsi, C. Portet, P. Simon and P.-L. Taberna, *Science*, 2006, **313**, 1760–1763.
18 J. Chmiola, C. Largeot, P.-L. Taberna, P. Simon and Y. Gogotsi, *Science*, 2010, **328**, 480–483.
19 Q. Wu, Y. Xu, Z. Yao, A. Liu and G. Shi, *ACS Nano*, 2010, **4**, 1963–1970.
20 H.-P. Cong, X.-C. Ren, P. Wang and S.-H. Yu, *Energy Environ. Sci.*, 2013, **6**, 1185–1191.
21 K. Jurewicz, S. Delpeux, V. Bertagna, F. Beguin and E. Frackowiak, *Chem. Phys. Lett.*, 2001, **347**, 36–40.
22 L. Yuan, B. Yao, B. Hu, K. Huo, W. Chen and J. Zhou, *Energy Environ. Sci.*, 2013, **6**, 470–476.
23 F. Alvi, M. K. Ram, P. A. Basnayaka, E. Stefanakos, Y. Goswami and A. Kumar, *Electrochim. Acta*, 2011, **56**, 9406–9412.
24 W. Wei, X. Cui, W. Chen and D. G. Ivey, *Chem. Soc. Rev.*, 2011, **40**, 1697–1721.
25 S. Chen, J. Zhu, X. Wu, Q. Han and X. Wang, *ACS Nano*, 2010, **4**, 2822–2830.
26 C. Yuan, X. Zhang, L. Su, B. Gao and L. Shen, *J. Mater. Chem.*, 2009, **19**, 5772–5777.
27 C.-C. Hu, K.-H. Chang, M.-C. Lin and Y.-T. Wu, *Nano Lett.*, 2006, **6**, 2690–2695.
28 Z. Chen, V. Augustyn, J. Wen, Y. Zhang, M. Shen, B. Dunn and Y. Lu, *Adv. Mater.*, 2011, **23**, 791–795.
29 A. Pandolfo and A. Hollenkamp, *J. Power Sources*, 2006, **157**, 11–27.
30 R. Kötz and M. Carlen, *Electrochim. Acta*, 2000, **45**, 2483–2498.
31 M. D. Stoller and R. S. Ruoff, *Energy Environ. Sci.*, 2010, **3**, 1294–1301.
32 L. Hu and Y. Cui, *Energy Environ. Sci.*, 2012, **5**, 6423–6435.
33 S. Park, M. Vosguerichian and Z. Bao, *Nanoscale*, 2013, **5**, 1727–1752.
34 Y. He, W. Chen, C. Gao, J. Zhou, X. Li and E. Xie, *Nanoscale*, 2013, **5**, 8799–8820.
35 T. Chen, H. Peng, M. Durstock and L. Dai, *Sci. Rep.*, 2014, **4**, 3612–3618.
36 B. G. Choi, J. Hong, W. H. Hong, P. T. Hammond and H. Park, *ACS Nano*, 2011, **5**, 7205–7213.
37 K. Novoselov, V. Fal, L. Colombo, P. Gellert, M. Schwab and K. Kim, *Nature*, 2012, **490**, 192–200.
38 S. Bose, T. Kuila, A. K. Mishra, R. Rajasekar, N. H. Kim and J. H. Lee, *J. Mater. Chem.*, 2012, **22**, 767–784.
39 H. Jiang, P. S. Lee and C. Li, *Energy Environ. Sci.*, 2013, **6**, 41–53.
40 Y. Cheng and J. Liu, *Mater. Res. Lett.*, 2013, **1**, 175–192.
41 C. Xu, B. Xu, Y. Gu, Z. Xiong, J. Sun and X. Zhao, *Energy Environ. Sci.*, 2013, **6**, 1388–1414.
42 L. L. Zhang, Y. Gu and X. S. Zhao, *J. Mater. Chem. A*, 2013, **1**, 9395–9408.
43 G. A. Snook, P. Kao and A. S. Best, *J. Power Sources*, 2011, **196**, 1–12.
44 K. Wang, H. Wu, Y. Meng and Z. Wei, *Small*, 2014, **10**, 14–31.
45 Z. S. Wu, K. Parvez, X. Feng and K. Müllen, *Nat. Commun.*, 2013, **4**, 2487–2494.
46 J. Bae, M. K. Song, Y. J. Park, J. M. Kim, M. Liu and Z. L. Wang, *Angew. Chem., Int. Ed.*, 2011, **50**, 1683–1687.
47 C. Yu, C. Masarapu, J. Rong, B. Wei and H. Jiang, *Adv. Mater.*, 2009, **21**, 4793–4797.
48 G. Wee, T. Salim, Y. M. Lam, S. G. Mhaisalkar and M. Srinivasan, *Energy Environ. Sci.*, 2011, **4**, 413–416.
49 M. F. El-Kady, V. Strong, S. Dubin and R. B. Kaner, *Science*, 2012, **335**, 1326–1330.
50 J. J. Yoo, K. Balakrishnan, J. Huang, V. Meunier, B. G. Sumpter, A. Srivastava, M. Conway, A. L. Mohana Reddy, J. Yu and R. Vajtai, *Nano Lett.*, 2011, **11**, 1423–1427.
51 F. Du, D. Yu, L. Dai, S. Ganguli, V. Varshney and A. Roy, *Chem. Mater.*, 2011, **23**, 4810–4816.
52 J. A. Lee, M. K. Shin, S. H. Kim, H. U. Cho, G. M. Spinks, G. G. Wallace, M. D. Lima, X. Lepró, M. E. Kozlov, R. H. Baughman and S. J. Kim, *Nat Commun.*, 2013, **4**, 1970–1977.
53 Z. Yang, J. Deng, X. Chen, J. Ren and H. Peng, *Angew. Chem., Int. Ed.*, 2013, **52**, 13453–13457.
54 T. Chen, L. Qiu, Z. Yang, Z. Cai, J. Ren, H. Li, H. Lin, X. Sun and H. Peng, *Angew. Chem., Int. Ed.*, 2012, **51**, 11977–11980.
55 T. Chen, Y. Xue, A. K. Roy and L. Dai, *ACS Nano*, 2014, **8**, 1039–1046.
56 Y. Zhao, J. Liu, Y. Hu, H. Cheng, C. Hu, C. Jiang, L. Jiang, A. Cao and L. Qu, *Adv. Mater.*, 2013, **25**, 591–595.
57 M. Kaempgen, C. K. Chan, J. Ma, Y. Cui and G. Gruner, *Nano Lett.*, 2009, **9**, 1872–1876.
58 L. Hu, M. Pasta, F. L. Mantia, L. Cui, S. Jeong, H. D. Deshazer, J. W. Choi, S. M. Han and Y. Cui, *Nano Lett.*, 2010, **10**, 708–714.

59 Y. J. Kang, H. Chung, C.-H. Han and W. Kim, *Nanotechnology*, 2012, **23**, 065401.
60 Y. J. Kang, S.-J. Chun, S.-S. Lee, B.-Y. Kim, J. H. Kim, H. Chung, S.-Y. Lee and W. Kim, *ACS Nano*, 2012, **6**, 6400–6406.
61 V. L. Pushparaj, M. M. Shaijumon, A. Kumar, S. Murugesan, L. Ci, R. Vajtai, R. J. Linhardt, O. Nalamasu and P. M. Ajayan, *Proc. Natl. Acad. Sci. U. S. A.*, 2007, **104**, 13574–13577.
62 C. Huang and P. S. Grant, *Sci. Rep.*, 2013, **3**, 2393–2401.
63 L. Hu, W. Chen, X. Xie, N. Liu, Y. Yang, H. Wu, Y. Yao, M. Pasta, H. N. Alshareef and Y. Cui, *ACS Nano*, 2011, **5**, 8904–8913.
64 G. Yu, X. Xie, L. Pan, Z. Bao and Y. Cui, *Nano Energy*, 2013, **2**, 213–234.
65 L. Nyholm, G. Nyström, A. Mihranyan and M. Strømme, *Adv. Mater.*, 2011, **23**, 3751–3769.
66 K. Wang, P. Zhao, X. Zhou, H. Wu and Z. Wei, *J. Mater. Chem.*, 2011, **21**, 16373–16378.
67 C. Meng, C. Liu, L. Chen, C. Hu and S. Fan, *Nano Lett.*, 2010, **10**, 4025–4031.
68 J. S. Ye, H. F. Cui, X. Liu, T. M. Lim, W. D. Zhang and F. S. Sheu, *Small*, 2005, **1**, 560–565.
69 H. Lin, L. Li, J. Ren, Z. Cai, L. Qiu, Z. Yang and H. Peng, *Sci. Rep.*, 2013, **3**, 1353–1358.
70 A. Ghosh, V. T. Le, J. J. Bae and Y. H. Lee, *Sci. Rep.*, 2013, **3**, 2939–2948.
71 L. Dai, A. Patil, X. Gong, Z. Guo, L. Liu, Y. Liu and D. Zhu, *ChemPhysChem*, 2003, **4**, 1150–1169.
72 W. Lu, L. Qu, K. Henry and L. Dai, *J. Power Sources*, 2009, **189**, 1270–1277.
73 S. Huang and L. Dai, *J. Phys. Chem. B*, 2002, **106**, 3543–3545.
74 H. Zhang, G. Cao, Z. Wang, Y. Yang, Z. Shi and Z. Gu, *Nano Lett.*, 2008, **8**, 2664–2668.
75 Q.-L. Chen, K.-H. Xue, W. Shen, F.-F. Tao, S.-Y. Yin and W. Xu, *Electrochim. Acta*, 2004, **49**, 4157–4161.
76 W. Lu, L. Qu, L. Dai and K. Henry, *ECS Trans.*, 2008, **6**, 257–261.
77 A. K. Geim and K. S. Novoselov, *Nat. Mater.*, 2007, **6**, 183–191.
78 A. K. Geim, *Science*, 2009, **324**, 1530–1534.
79 L. Dai, *Acc. Chem. Res.*, 2012, **46**, 31–42.
80 D. Li, M. B. Mueller, S. Gilje, R. B. Kaner and G. G. Wallace, *Nat. Nanotechnol.*, 2008, **3**, 101–105.
81 G. Eda, G. Fanchini and M. Chhowalla, *Nat. Nanotechnol.*, 2008, **3**, 270–274.
82 J. N. Coleman, M. Lotya, A. O'Neill, S. D. Bergin, P. J. King, U. Khan, K. Young, A. Gaucher, S. De and R. J. Smith, *Science*, 2011, **331**, 568–571.
83 X. Li, W. Cai, J. An, S. Kim, J. Nah, D. Yang, R. Piner, A. Velamakanni, I. Jung and E. Tutuc, *Science*, 2009, **324**, 1312–1314.
84 I.-Y. Jeon, Y.-R. Shin, G.-J. Sohn, H.-J. Choi, S.-Y. Bae, J. Mahmood, S.-M. Jung, J.-M. Seo, M.-J. Kim, D. W. Chang, L. Dai and J.-B. Baek, *Proc. Natl. Acad. Sci. U. S. A.*, 2012, **109**, 5588–5593.
85 Y. Zhu, S. Murali, M. D. Stoller, K. Ganesh, W. Cai, P. J. Ferreira, A. Pirkle, R. M. Wallace, K. A. Cychosz, M. Thommes, D. Su, E. A. Stach and R. S. Ruoff, *Science*, 2011, **332**, 1537–1541.
86 B. G. Choi, S.-J. Chang, H.-W. Kang, C. P. Park, H. J. Kim, W. H. Hong, S. Lee and Y. S. Huh, *Nanoscale*, 2012, **4**, 4983–4988.
87 J. Luo, H. D. Jang, T. Sun, L. Xiao, Z. He, A. P. Katsoulidis, M. G. Kanatzidis, J. M. Gibson and J. Huang, *ACS Nano*, 2011, **5**, 8943–8949.
88 M. D. Stoller, S. Park, Y. Zhu, J. An and R. S. Ruoff, *Nano Lett.*, 2008, **8**, 3498–3502.
89 Z. Chen, W. Ren, L. Gao, B. Liu, S. Pei and H.-M. Cheng, *Nat. Mater.*, 2011, **10**, 424–428.
90 Y. Xu, K. Sheng, C. Li and G. Shi, *ACS Nano*, 2010, **4**, 4324–4330.
91 K.-X. Sheng, Y.-X. Xu, C. Li and G.-Q. Shi, *New Carbon Mater.*, 2011, **26**, 9–15.
92 L. Zhang and G. Shi, *J. Phys. Chem. C*, 2011, **115**, 17206–17212.
93 J. Chen, K. Sheng, P. Luo, C. Li and G. Shi, *Adv. Mater.*, 2012, **24**, 4569–4573.
94 X. Zhang, Z. Sui, B. Xu, S. Yue, Y. Luo, W. Zhan and B. Liu, *J. Mater. Chem.*, 2011, **21**, 6494–6497.
95 Z. S. Wu, A. Winter, L. Chen, Y. Sun, A. Turchanin, X. Feng and K. Müllen, *Adv. Mater.*, 2012, **24**, 5130–5135.
96 Y. Xue, J. Liu, H. Chen, R. Wang, D. Li, J. Qu and L. Dai, *Angew. Chem., Int. Ed.*, 2012, **51**, 12124–12127.
97 Y. Xue, D. Yu, L. Dai, R. Wang, D. Li, A. Roy, F. Lu, H. Chen, Y. Liu and J. Qu, *Phys. Chem. Chem. Phys.*, 2013, **15**, 12220–12226.
98 Y. Xu, Z. Lin, X. Huang, Y. Liu, Y. Huang and X. Duan, *ACS Nano*, 2013, **7**, 4042–4049.
99 I.-Y. Jeon, H.-J. Choi, S.-M. Jung, J.-M. Seo, M.-J. Kim, L. Dai and J.-B. Baek, *J. Am. Chem. Soc.*, 2012, **135**, 1386–1393.
100 I. Y. Jeon, S. Zhang, L. Zhang, H. J. Choi, J. M. Seo, Z. Xia, L. Dai and J. B. Baek, *Adv. Mater.*, 2013, **25**, 6138–6145.
101 I.-Y. Jeon, H.-J. Choi, M. J. Ju, I. T. Choi, K. Lim, J. Ko, H. K. Kim, J. C. Kim, J.-J. Lee, D. Shin, S.-M. Jung, J.-M. Seo, M.-J. Kim, N. Park, L. Dai and J.-B. Baek, *Sci. Rep.*, 2013, **3**, 2260–2266.
102 I.-Y. Jeon, H.-J. Choi, M. Choi, J.-M. Seo, S.-M. Jung, M.-J. Kim, S. Zhang, L. Zhang, Z. Xia, L. Dai, N. Park and J.-B. Baek, *Sci. Rep.*, 2013, **3**, 1810–1816.
103 D. Yu and L. Dai, *J. Phys. Chem. Lett.*, 2009, **1**, 467–470.
104 Y. Cheng, S. Lu, H. Zhang, C. V. Varanasi and J. Liu, *Nano Lett.*, 2012, **12**, 4206–4211.
105 S.-Y. Yang, K.-H. Chang, H.-W. Tien, Y.-F. Lee, S.-M. Li, Y.-S. Wang, J.-Y. Wang, C.-C. M. Ma and C.-C. Hu, *J. Mater. Chem.*, 2011, **21**, 2374–2380.
106 Z.-D. Huang, B. Zhang, S.-W. Oh, Q.-B. Zheng, X.-Y. Lin, N. Yousefi and J.-K. Kim, *J. Mater. Chem.*, 2012, **22**, 3591–3599.
107 H. Gao, F. Xiao, C. B. Ching and H. Duan, *ACS Appl. Mater. Interfaces*, 2012, **4**, 7020–7026.
108 G. K. Dimitrakakis, E. Tylianakis and G. E. Froudakis, *Nano Lett.*, 2008, **8**, 3166–3170.
109 Y. Mao and J. Zhong, *New J. Phys.*, 2009, **11**, 093002.

110 V. Varshney, S. S. Patnaik, A. K. Roy, G. Froudakis and B. L. Farmer, *ACS Nano*, 2010, **4**, 1153–1161.
111 E. F. Sheka and L. A. Chernozatonskii, *J. Comput. Theor. Nanosci.*, 2010, **7**, 1814–1824.
112 J. Arellano, *J. Nano Res.*, 2009, **5**, 201–211.
113 O. Barbieri, M. Hahn, A. Herzog and R. Kötz, *Carbon*, 2005, **43**, 1303–1310.
114 H. Wang, H. S. Casalongue, Y. Liang and H. Dai, *J. Am. Chem. Soc.*, 2010, **132**, 7472–7477.
115 J. Lin, C. Zhang, Z. Yan, Y. Zhu, Z. Peng, R. H. Hauge, D. Natelson and J. M. Tour, *Nano Lett.*, 2012, **13**, 72–78.
116 D. Pech, M. Brunet, H. Durou, P. Huang, V. Mochalin, Y. Gogotsi, P.-L. Taberna and P. Simon, *Nat. Nanotechnol.*, 2010, **5**, 651–654.
117 J.-H. Sung, S.-J. Kim, S.-H. Jeong, E.-H. Kim and K.-H. Lee, *J. Power Sources*, 2006, **162**, 1467–1470.
118 W. Gao, N. Singh, L. Song, Z. Liu, A. L. M. Reddy, L. Ci, R. Vajtai, Q. Zhang, B. Wei and P. M. Ajayan, *Nat. Nanotechnol.*, 2011, **6**, 496–500.
119 K. Wang, W. Zou, B. Quan, A. Yu, H. Wu, P. Jiang and Z. Wei, *Adv. Energy Mater.*, 2011, **1**, 1068–1072.
120 M. Xue, Z. Xie, L. Zhang, X. Ma, X. Wu, Y. Guo, W. Song, Z. Li and T. Cao, *Nanoscale*, 2011, **3**, 2703–2708.
121 Z. Niu, L. Zhang, L. Liu, B. Zhu, H. Dong and X. Chen, *Adv. Mater.*, 2013, **25**, 4035–4042.
122 M. F. El-Kady and R. B. Kaner, *Nat. Commun.*, 2013, **4**, 1475–1482.
123 L. Bao and X. Li, *Adv. Mater.*, 2012, **24**, 3246–3252.
124 W.-W. Liu, X.-B. Yan, J.-W. Lang, C. Peng and Q.-J. Xue, *J. Mater. Chem.*, 2012, **22**, 17245–17253.
125 T. Chen, L. Qiu, Z. Yang and H. Peng, *Chem. Soc. Rev.*, 2013, **42**, 5031–5041.
126 Y. Fu, X. Cai, H. Wu, Z. Lv, S. Hou, M. Peng, X. Yu and D. Zou, *Adv. Mater.*, 2012, **24**, 5713–5718.
127 X. Xiao, T. Li, P. Yang, Y. Gao, H. Jin, W. Ni, W. Zhan, X. Zhang, Y. Cao and J. Zhong, *ACS Nano*, 2012, **6**, 9200–9206.
128 J. Ren, L. Li, C. Chen, X. Chen, Z. Cai, L. Qiu, Y. Wang, X. Zhu and H. Peng, *Adv. Mater.*, 2013, **25**, 1155–1159.
129 Y. Meng, Y. Zhao, C. Hu, H. Cheng, Y. Hu, Z. Zhang, G. Shi and L. Qu, *Adv. Mater.*, 2013, **25**, 2326–2331.
130 Z. Cai, L. Li, J. Ren, L. Qiu, H. Lin and H. Peng, *J. Mater. Chem. A*, 2013, **1**, 258–261.
131 K. Wang, Q. Meng, Y. Zhang, Z. Wei and M. Miao, *Adv. Mater.*, 2013, **25**, 1494–1498.
132 J. A. Rogers, T. Someya and Y. Huang, *Science*, 2010, **327**, 1603–1607.
133 S. H. Chae, W. J. Yu, J. J. Bae, D. L. Duong, D. Perello, H. Y. Jeong, Q. H. Ta, T. H. Ly, Q. A. Vu, M. Yun, X. Duan and Y. H. Lee, *Nat. Mater.*, 2013, **12**, 403–409.
134 Z. Yu, X. Niu, Z. Liu and Q. Pei, *Adv. Mater.*, 2011, **23**, 3989–3994.
135 D. J. Lipomi, B. C. K. Tee, M. Vosgueritchian and Z. Bao, *Adv. Mater.*, 2011, **23**, 1771–1775.
136 M. S. White, M. Kaltenbrunner, E. D. Glowacki, K. Gutnichenko, G. Kettlgruber, I. Graz, S. Aazou, C. Ulbricht, D. A. M. Egbe, M. C. Miron, Z. Major, M. C. Scharber, T. Sekitani, T. Someya, S. Bauer and N. S. Sariciftci, *Nat. Photonics*, 2013, **7**, 811–816.
137 S. Xu, Y. Zhang, J. Cho, J. Lee, X. Huang, L. Jia, J. A. Fan, Y. Su, J. Su, H. Zhang, H. Cheng, B. Lu, C. Yu, C. Chuang, T.-i. Kim, T. Song, K. Shigeta, S. Kang, C. Dagdeviren, I. Petrov, P. V. Braun, Y. Huang, U. Paik and J. A. Rogers, *Nat Commun.*, 2013, **4**, 1543–1550.
138 Z. Niu, H. Dong, B. Zhu, J. Li, H. H. Hng, W. Zhou, X. Chen and S. Xie, *Adv. Mater.*, 2013, **25**, 1058–1064.
139 X. Li, T. Gu and B. Wei, *Nano Lett.*, 2012, **12**, 6366–6371.
140 C. Zhao, C. Wang, Z. Yue, K. Shu and G. G. Wallace, *ACS Appl. Mater. Interfaces*, 2013, **5**, 9008–9014.
141 M. W. Rowell and M. D. McGehee, *Energy Environ. Sci.*, 2011, **4**, 131–134.
142 A. Colsmann, A. Puetz, A. Bauer, J. Hanisch, E. Ahlswede and U. Lemmer, *Adv. Energy Mater.*, 2011, **1**, 599–603.
143 Y. H. Kim, J. Lee, S. Hofmann, M. C. Gather, L. Müller-Meskamp and K. Leo, *Adv. Funct. Mater.*, 2013, **23**, 3763–3769.
144 Y. Yang, S. Jeong, L. Hu, H. Wu, S. W. Lee and Y. Cui, *Proc. Natl. Acad. Sci. U. S. A.*, 2011, **108**, 13013–13018.
145 Z. Niu, W. Zhou, J. Chen, G. Feng, H. Li, Y. Hu, W. Ma, H. Dong, J. Li and S. Xie, *Small*, 2013, **9**, 518–524.
146 H. Y. Jung, M. B. Karimi, M. G. Hahm, P. M. Ajayan and Y. J. Jung, *Sci. Rep.*, 2012, **2**, 773–777.
147 A. Yu, I. Roes, A. Davies and Z. Chen, *Appl. Phys. Lett.*, 2010, **96**, 253105.
148 K. S. Kim, Y. Zhao, H. Jang, S. Y. Lee, J. M. Kim, K. S. Kim, J.-H. Ahn, P. Kim, J.-Y. Choi and B. H. Hong, *Nature*, 2009, **457**, 706–710.
149 S. Bae, H. Kim, Y. Lee, X. Xu, J.-S. Park, Y. Zheng, J. Balakrishnan, T. Lei, H. Ri Kim, Y. I. Song, Y.-J. Kim, K. S. Kim, B. Ozyilmaz, J.-H. Ahn, B. H. Hong and S. Iijima, *Nat. Nanotechnol.*, 2010, **5**, 574–578.
150 X. Li, Y. Zhu, W. Cai, M. Borysiak, B. Han, D. Chen, R. D. Piner, L. Colombo and R. S. Ruoff, *Nano Lett.*, 2009, **9**, 4359–4363.
151 T. Chen, Z. Yang and H. Peng, *ChemPhysChem*, 2013, **14**, 1777–1782.
152 Y.-H. Lee, J.-S. Kim, J. Noh, I. Lee, H. J. Kim, S. Choi, J. Seo, S. Jeon, T.-S. Kim, J.-Y. Lee and J. W. Choi, *Nano Lett.*, 2013, **13**, 5753–5761.
153 W. Guo, X. Xue, S. Wang, C. Lin and Z. L. Wang, *Nano Lett.*, 2012, **12**, 2520–2523.
154 T. N. Murakami, N. Kawashima and T. Miyasaka, *Chem. Commun.*, 2005, 3346–3348.
155 Z. Yang, L. Li, Y. Luo, R. He, L. Qiu, H. Lin and H. Peng, *J. Mater. Chem. A*, 2013, **1**, 954–958.
156 J. Bae, Y. J. Park, M. Lee, S. N. Cha, Y. J. Choi, C. S. Lee, J. M. Kim and Z. L. Wang, *Adv. Mater.*, 2011, **23**, 3446–3449.
157 Y. Fu, H. Wu, S. Ye, X. Cai, X. Yu, S. Hou, H. Kafafy and D. Zou, *Energy Environ. Sci.*, 2013, **6**, 805–812.
158 Z. Zhang, X. Chen, P. Chen, G. Guan, L. Qiu, H. Lin, Z. Yang, W. Bai, Y. Luo and H. Peng, *Adv. Mater.*, 2014, **26**, 466–470.

